Macrocephaly, Increased Intracranial Pressure, and Hydrocephalus in the Infant and Young Child

Alexandra T. Vertinsky, MD and Patrick D. Barnes, MD

Abstract: Macrocephaly, increased intracranial pressure, and hydrocephalus are common related conditions that lead to cross-sectional imaging of the infant and young child. Imaging plays a central role in establishing the diagnosis and guiding disposition and treatment of these patients. In this review, a general overview is provided, and the more common causes of hydrocephalus are presented, including posthemorrhage, postinfection, developmental malformations, and masses. Imaging guidelines are also outlined for initial evaluation and follow-up, along with a discussion of the imaging features of shunt malfunction.

Key Words: macrocephaly, hydrocephalus, pediatric, MRI

(*Top Magn Reson Imaging* 2007;18:31–51)

Macrocephaly (MC), increased intracranial pressure (ICP), and hydrocephalus (HC) are common related conditions that lead to cross-sectional imaging of the infant and young child. Imaging plays a central role in establishing the diagnosis and guiding disposition and treatment of these patients. In this review, a general overview is provided, and the more common causes of HC are presented, including posthemorrhage, postinfection, developmental malformations, and masses (Tables 1, 2). Imaging guidelines are also outlined for initial evaluation and follow-up, along with a discussion of the imaging features of shunt malfunction.

MACROCEPHALY

Macrocephaly is defined as a head circumference more than 2 SD above the mean. Common causes of MC include familial megalencephaly (larger-than-normal brain mass), benign extracerebral collections of infancy (BECC) and HC. Macrocephaly without HC may also be seen in some genetic, metabolic, and dysplastic syndromes, or may be caused by tumors and cysts, pseudotumor cerebri, or subdural collections (eg, hematomas, hygromas).[1] Evaluation of head growth rate (ie, serial head circumferences) along with assessment of developmental milestones, perinatal history, and signs of ICP is important for differential diagnosis, urgency of imaging, and radiological interpretation.[2]

Macrocephaly with normal growth rate and normal neurological examination is reassuring and is characteristic of benign megalencephaly, which is usually familial. Dysplastic megalencephaly is often associated with developmental delay, seizures, a neurocutaneous syndrome (eg, neurofibromatosis), a genetic syndrome (eg, Soto syndrome), hemimegalencephaly (Fig. 1), or elevated venous pressure (eg, achondroplasia) (Fig. 2). Macrocephaly from "rebound" or "catch-up" brain growth occurs in the thriving infant after prematurity or after a period of deprivation or serious illness. Familial, dysplastic, and rebound types of MC may manifest mild to moderate degrees of ventricular or subarachnoid space dilatation.[3–5]

MC and accelerated head growth without elevated pressure and with normal neurological exam may occur as nonprogressive subarachnoid space dilatation with or without ventricular enlargement. This pattern is most commonly referred to as BECC, but has also been termed as "benign enlargement of the subarachnoid spaces," "benign infantile HC," and "benign external HC."[1,3–7] The cause is unknown, but it may be related to delayed development of parasagittal dural channels responsible for cerebrospinal fluid (CSF) resorption in young children (who have few arachnoid villi). Accelerated head growth may continue until 12 to 18 months of age and then usually stabilizes as a form of megalencephaly. Imaging features of BECC include normal to mildly enlarged lateral and third ventricles and symmetric enlargement of the frontal subarachnoid spaces, interhemispheric fissure, and Sylvian fissures (Fig. 3).[4] These extracerebral collections must be differentiated from subdural collections. On magnetic resonance imaging (MRI), the visualization of 2 layers of differing signal intensity or of abnormal signal intensity related to blood products, rather than CSF, is helpful to identify subdural collections (Fig. 4).[5] The presence of bridging cortical draining veins extending through an extra-axial collection is supportive of, but not specific for, the subarachnoid space.[7] Infants with BECC may be at increased risk of subdural hematoma, spontaneously or from minor trauma, resulting from the stretching of cortical veins.[6,8]

MC with accelerated head growth due to progressive HC is usually associated with signs of ICP and often with declining milestones. The exception may be an infant or child with preexisting brain injury such as the premature infant with HC from intraventricular hemorrhage and coexistent periventricular leukomalacia (PVL). Other causes of MC with megalencephaly, hydrocephaly, or craniomegaly (enlarged calvarium) include lipid storage disease, leukodystrophies, cranial dysplasias, and marrow hyperplasia secondary to chronic hemolytic anemia.

INCREASED ICP

Symptoms and signs of ICP, depending on age, include MC, accelerating head circumference, full or bulging

From the Stanford University Medical Center, Stanford, CA.
Reprints: Patrick D. Barnes, MD, Departments of Radiology, Pediatric MRI and CT, Room 0511, Lucille Packard Children's Hospital, 725 Welch Road, Palo Alto, CA 94304 (e-mail: pbarnes@stanford.edu).
Copyright © 2007 by Lippincott Williams & Wilkins

Copyright © Lippincott Williams & Wilkins. Unauthorized reproduction of this article is prohibited.

TABLE 1. Overview of Clinical Presentations

Macrocephaly – head circumference more than two standard deviations above normal (ie, above 95 percentile)
Assess Clinical Parameters Head Growth Rate (serial head circumferences) Developmental milestones Signs of Raised ICP
-Normal growth rate and normal neurological exam **->Familial megalencephaly** (enlarged brain)
-Increased growth rate after illness/prematurity (eg, thriving infant after prematurity or illness) **->Rebound brain growth**
-Increased growth rate with normal neurological exam, normal developmental milestones **->Benign extracerebral collections of infancy**
-Abnormal neurological exam, developmental delay, seizures, genetic syndrome, systemic disease, etc. **->Dysplastic megalencephaly, metabolic disorders, anemias, cranial dysplasias, etc.**
-Macrocephaly with accelerated heady growth and signs of increased pressure **->Hydrocephalus**

fontanelle, split sutures, poor feeding, vomiting, irritability, vision impairment, headache, lethargy, stupor, encephalopathy, Parinaud syndrome, sixth nerve palsy, hypertonia with hyperreflexia, and papilledema.[9,10] The causes of ICP include trauma, hemorrhage, acute hypoxic-ischemic insult, infection, parainfectious sequela, metabolic derangement, HC, tumors, pseudotumor cerebri, and universal craniosynostosis.[9–16] Imaging is indicated to define a mass, fluid collection, edema, or HC. The mass may be a cyst, neoplasm, abscess, or hematoma. The abnormal fluid collection may be subdural or epidural, whether a hematoma, empyema, effusion, or hygroma. Edema may be traumatic (Fig. 5), hypoxic-ischemic (Fig. 6), toxic (eg, lead poisoning), metabolic (eg, ketoacidosis), infectious (meningitis or encephalitis), parainfectious (acute disseminated encephalomyelitis, Reye syndrome), or due to pseudotumor.

HYDROCEPHALUS

A common cause of MC and ICP in childhood is HC. Hydrocephalus is the state of excessive CSF volume with progressive enlargement of the ventricles, subarachnoid spaces, or both.[17–20] Hydrocephalus may be caused by an imbalance between CSF production and absorption, by a blockage of CSF flow, or from alterations in ventricular compliance and CSF pulse pressure.[17,20] Hydrocephalus due

TABLE 2. Macrocephaly, ICP, and HC

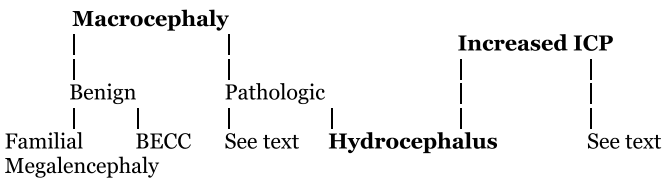

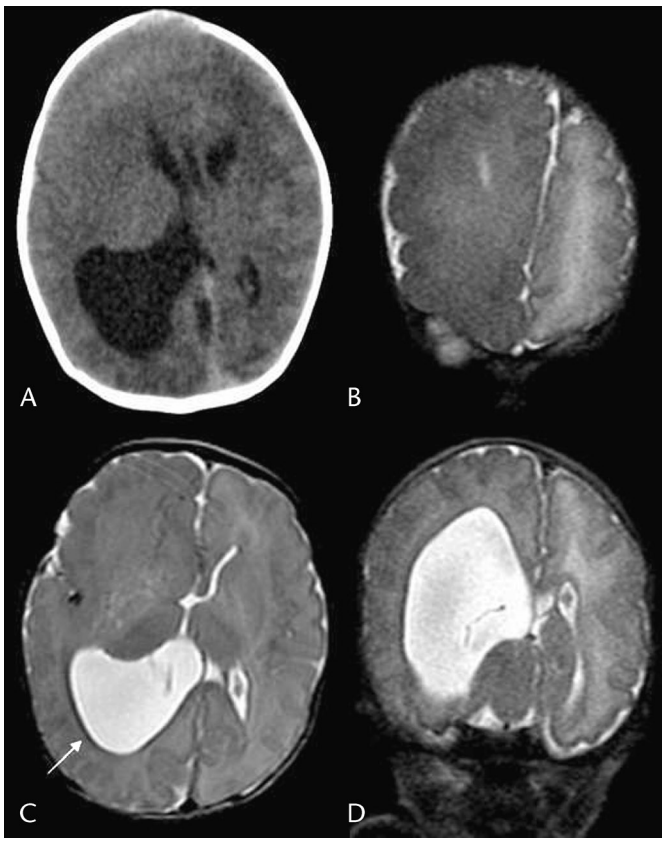

FIGURE 1. Hemimegalencephaly with macrocephaly and epilepsy. Prenatal US showed ventriculomegaly. Axial noncontrast CT at 2 days of life shows enlarged right cerebral hemisphere with a large dysplastic right lateral ventricle and thickened cortex (A). Axial T2 images (B, C) and coronal short τ inversion recovery (D) demonstrate enlargement of the right hemisphere and lateral ventricle, prominent trigone (white arrow) and occipital horn, and thickened gyri.

to CSF overproduction is very rare but may occur with choroid plexus papilloma (CPP) or villus hypertrophy. Hydrocephalus due to CSF flow block or absorptive block may be described as "communicating" when the block occurs outside the ventricular system (eg, basal cisterns or parasagittal arachnoid villi) and "noncommunicating" when there is intraventricular obstruction (at or proximal to the fourth ventricular outlets).[9,18]

Most childhood HC occurs in infancy (Table 3). The most common cause is acquired adhesive ependymitis or arachnoiditis after hemorrhage or infection.[9,17,18] Hydrocephalus is a well-known sequela of neonatal intracranial hemorrhage especially in the preterm (PT).[16] Prenatal or postnatal infection may also lead to HC.[11,12] By far the most common developmental cause of HC is the Chiari II malformation associated with myelocele/myelomeningocele (MMC). The HC often develops, or progresses, after repair of the spinal defect.[9,21] Other common developmental causes include aqueductal anomalies (forking, stenosis, septation, gliosis) and the Dandy-Walker-Blake spectrum of retrocerebellar cysts.[22] Less common or rare causes of HC include

© 2007 Lippincott Williams & Wilkins

Copyright © Lippincott Williams & Wilkins. Unauthorized reproduction of this article is prohibited.

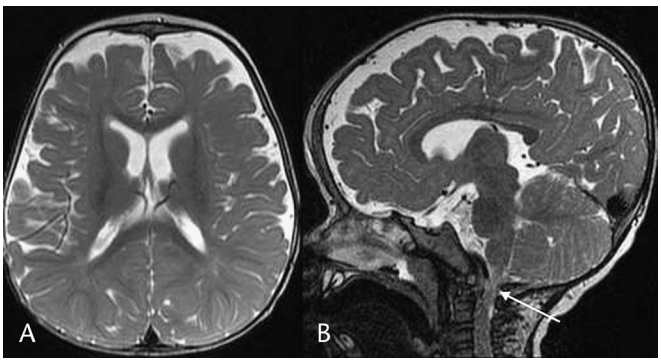

FIGURE 2. Achondroplasia. Axial T2 image shows mild prominence of the lateral ventricles and enlarged subarachnoid spaces (A). Sagittal T2 (B) image show a small skull base and small foramen magnum (white arrow).

foramen of Monro atresia, skull base anomalies, intracranial cyst, craniosynostosis, encephalocele (Fig. 7), holoprosencephaly (Fig. 8), hydranencephaly, and lissencephaly (Fig. 9).[23]

IMAGING EVALUATION

The imaging diagnosis of HC may be made with ultrasonography (US), computed tomography (CT), or MRI. Although ventricular enlargement in the absence of atrophy or underdevelopment suggests HC, this finding alone may not be specific. Clinical features of ICP or progressive head enlargement supports the diagnosis of HC. Additional imaging features supportive of HC include ballooned enlargement of the anterior and posterior recesses of the third ventricle, rounded configuration of the lateral ventricles with decreased ventricular angles, accentuated CSF flow voids on MRI, and dilatation of the temporal horns proportionate with that of the lateral ventricle bodies.[6,9,24–26] Disproportionate enlargement of ventricles relative to sulci is not as reliable in differentiating underdevelopment or atrophy from HC in infants and young children. Periventricular edema due to transependymal CSF flow or hydrostatic stasis from elevated intraventricular pressure may be evident as blurred or ill-defined ventricular margins. This finding favors acute/subacute or progressive HC (Figs. 10, 11). However, the normally high water content of the immature white matter may obscure edema due to HC in the infant.[6,9,24–26]

Hydrocephalus in the fetus and infant is often diagnosed with US or CT initially.[9,27] Doppler US using the graded fontanelle compression technique may be used to identify infants with ventriculomegaly and ICP, and help determine the need and timing for shunting.[28] Magnetic resonance imaging may be indicated to further delineate HC when surgery is more specifically directed beyond that of simple shunting, as may occur in the setting of a retrocerebellar cyst, isolation of the fourth ventricle, porencephaly, postventriculitis encystment, or a ventricular tumor.[9,25,26] Proper catheter placement for management of HC related to a cyst in the Dandy-Walker-Blake spectrum (ie, shunting of the cyst, the ventricles, or both) often depends upon patency of the aqueduct. Upward or downward herniation may occur due to unbalanced decompression of the ventricles relative to the cyst.[9,22] Magnetic resonance imaging has an important role in planning the surgical management of these cases.

Endoscopic third ventriculostomy (ETV) is a relatively new neurosurgical procedure. It is often used for patients with obstruction at or distal to the posterior third ventricle who have patent subarachnoid spaces. The obstruction is bypassed by a surgical opening made in the floor. Endoscopic third ventriculostomy has been used in children primarily for decompression of HC due to aqueductal stenosis in the absence of communicating HC or immaturity of the arachnoid villi.[17,29,30] More recently, it has undergone evaluation for treating other etiologies of HC.[31–37] Although ETV is still considered to be more effective in patients older than 2 years, it is being advocated in younger patients. The success rate is enhanced in infants with a defined anatomic obstruction. However, moderate success (~40%–60%) has

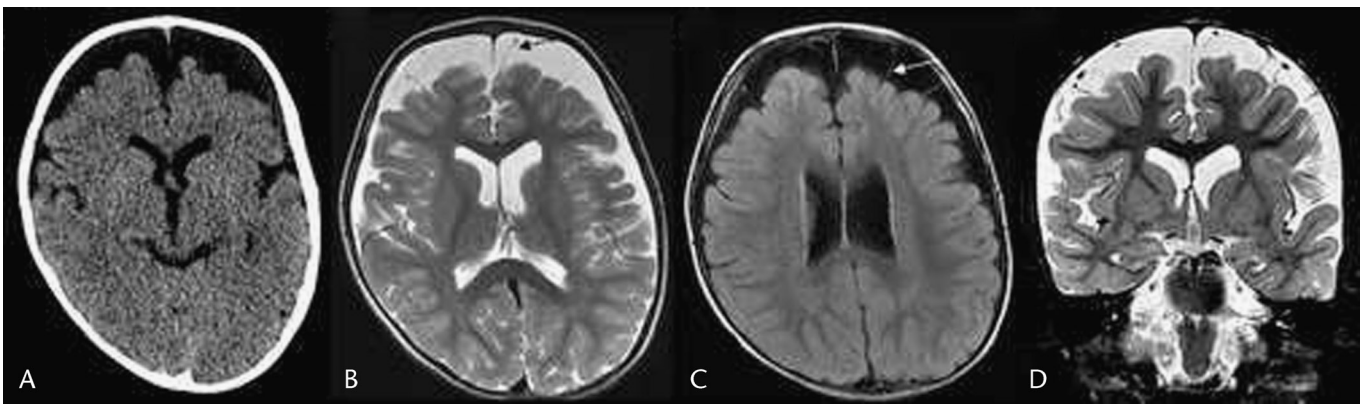

FIGURE 3. Benign extracerebral collections of infancy. A, Noncontrast computed tomographic images demonstrate normal brain densities with prominent frontal subarachnoid spaces bilaterally and slight widening of the ventricles and sylvian fissures. B–D, Magnetic resonance imaging in another infant. Axial T2 (B) and FLAIR (C) plus coronal short τ inversion recovery (D) images demonstrate linear cortical veins (arrows) traversing the enlarged extracerebral spaces that conform to CSF intensities on all sequences.

© 2007 Lippincott Williams & Wilkins

Copyright © Lippincott Williams & Wilkins. Unauthorized reproduction of this article is prohibited.

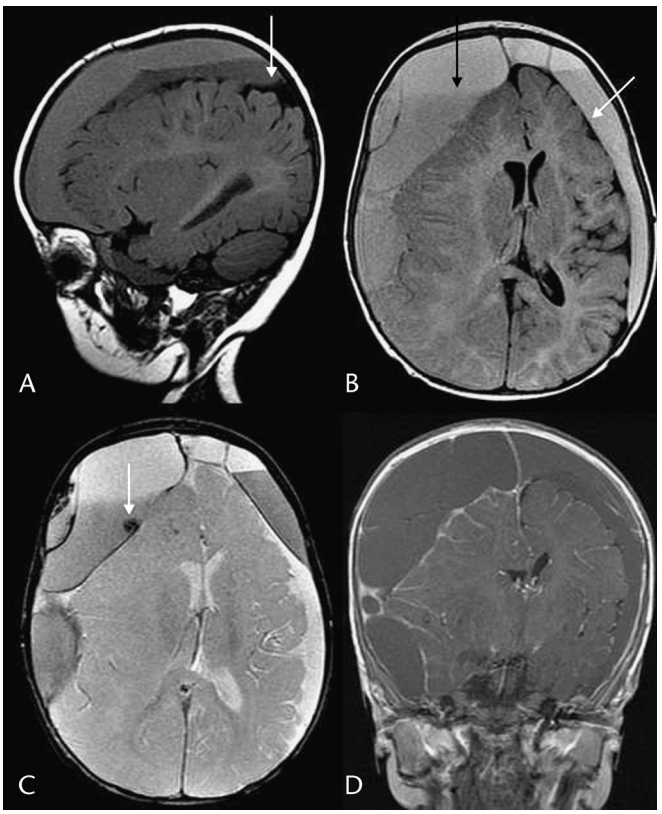

FIGURE 4. Subdural hematomas in a 5-month-old boy with macrocephaly and seizures**.** Magnetic resonance imaging demonstrates loculated subdural hematomas with blood products of differing ages. A, Sagittal T1 image shows mixed-intensity subdural collections consistent with acute (or possibly hyperacute) hemorrhage. Note the line separating the collection from the low-intensity subarachnoid space (white arrow). B, Axial FLAIR image shows the separation of the collection from the subarachnoid space (especially over the left convexity, white arrow). The collections have mixed high intensity with fluid-fluid levels (black arrow) and septations present. Cortical veins are not seen crossing the collections. There is mass effect with right to left shift. C, Axial gradient echo (GRE) image shows susceptibility with hypointensities along the septations (white arrow). D, Coronal postgadolinium T1 image shows enhancement of the cortical vessels, and margins of the collections, but no traversing veins.

been documented for infants with posthemorrhagic or postinfectious HC, as well as for HC associated with MMC and Chiari II.[31] Magnetic resonance imaging facilitates surgical planning by delineating the anatomy of the third ventricle, the prepontine cistern, and the course of the basilar artery. It also assists in the assessment of ETV patency after surgery.[38]

Although CT may be a practical screening examination for HC after infancy, MRI is preferred because neoplasm becomes the leading consideration.[9] The superior contrast resolution, multiplanar imaging capability, and ability to assess parameters such as flow and tissue anisotropy make MR I the procedure of choice for delineation of anatomy and extent of tumor for planning of surgery, radiotherapy, and chemotherapy, as well as for follow-up of tumor response and treatment effects. Magnetic resonance imaging may offer more supportive or causative information when the CT or US demonstrate nonspecific ventriculomegaly. Unexplained HC requires a thorough investigation for an occult inflammatory or neoplastic process.[9] Magnetic resonance imaging may demonstrate a periaqueductal tumor in "presumed" aqueductal stenosis or leptomeningeal enhancement in inflammatory or neoplastic infiltration (eg, due to granulomatous infection or tumor seeding). Magnetic resonance imaging may also clarify nonspecific extracerebral collections first identified on CT or US by differentiating benign infantile extracerebral collections from subdural hematomas as discussed earlier.[4,5,9,14]

Follow-Up Evaluation

Treatment of HC involves the resection or decompression of the causative mass, ventricular diversion, or both.[9,13,19,30] Prognosis depends on the origin of the HC and on timing of the treatment. The prognosis for HC associated with an extensive brain malformation or diffuse brain injury is poor. The secondary effects of HC on the malformed, injured, or developing brain may be devastating. Unchecked progressive HC produces interstitial edema, ependymal disruption, spontaneous ventriculostomy, possible herniation, and subependymal gliosis, demyelination, cystic leukomalacia, neuronal injury, and atrophy.[9,17,29,30] The goal of shunting is to reduce pressure to safe levels and to protect brain tissue. Successful shunting is demonstrated on follow-up imaging as a proportionate decrease in ventricular size and reestablishment of brain mantle thickness (Fig. 12).[9,29,30]

The follow-up imaging of shunted (eg, ventriculoperitoneal [VP]), nonneoplastic HC may be adequately done with US or CT.[27] Ultrasonography is also an ideal guide for shunt placement intraoperatively and for shunt placement evaluation on follow-up. After loss of the acoustic window in older infants and children, CT becomes the procedure of choice for routine follow-up and for evaluating shunt complications, including malfunction and subdural fluid collections.[9] Magnetic resonance imaging provides multiplanar anatomical and multiparametric delineation, including CSF flow dynamics, which can be helpful for assessment of complex, compartmentalized, or encysted HC.[9,20,25,26] In general, after ETV, ventricular size decreases more slowly and to a lesser degree than seen after shunt placement.[38–40] Visualization of flow through the third ventriculostomy by MRI along with demonstration of a moderate decrease in ventricular size correlates with ETV success.[38,39] Ventriculostomy patency is assessed using a thin-slice sagittal T2 fast spin echo sequence. Visualization of a CSF flow-void in the third ventricular floor extending to the suprasellar cistern is an indicator of shunt patency (Fig. 13).[41]

SPECIFIC CAUSES OF HC IN CHILDHOOD

Posthemorrhagic HC and Venous Hypertension

Germinal matrix (GM)/intraventricular hemorrhage (IVH), which occurs in 20% of infants born before 34 weeks'

© 2007 Lippincott Williams & Wilkins

Copyright © Lippincott Williams & Wilkins. Unauthorized reproduction of this article is prohibited.

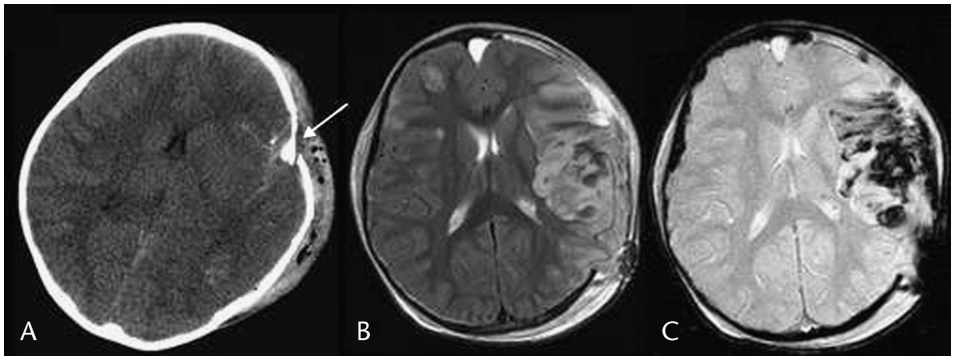

FIGURE 5. Traumatic injury in a 2-year-old boy struck by a car. A, Noncontrast CT shows left depressed skull fractures (white arrow), frontal and temporal cerebral edema with loss of gray-white matter differentiation, hemorrhages, and mass effect (posttraumatic infarction or contusion). A left hemicraniectomy was done for impending herniation. Postcraniectomy axial T2 (B) and GRE (C) images show increased hemorrhage and gyral swelling mainly in the left MCA distribution with transcraniectomy herniation. This is more consistent with infarction than with contusion.

gestation, is one of the most common severe complications among PT and low-birth-weight infants and often results in HC.[42] Germinal matrix/IVH is the sequela of a combination of intravascular, vascular, and extravascular factors that are related to prenatal, natal, and postnatal events. Intravascular factors include changes in cerebral blood flow or central nervous system (CNS) blood pressure that arise from elevated cerebral venous pressure due to mechanical ventilation, barotrauma, apnea, sepsis, or congestive heart failure. Vascular and extravascular factors refer to fragility of vessels in the GM, the site of origin of neuronal and glial cells destined for cortex. In the premature infant, matrix vessels are susceptible to rupture and hemorrhage due to the lack of structural elements that are present in more mature vessels and due to the lack of adequate external tissue support. The severity of GM hemorrhage is typically graded with increasing severity from I to IV. Grade I is subependymal hemorrhage confined to the GM (caudothalamic groove). Grade II denotes intraventricular extension without ventricular dilatation. Grade III is subependymal and intraventricular hemorrhage with HC (Fig. 14). Grade IV refers to additional hemorrhagic periventricular infarction resulting from subependymal venous occlusion. Poor neurodevelopmental outcome in PT brain injury generally correlates with the higher grades of GM/IVH, parenchymal injury (eg, PVL), and ventriculomegaly.[42,43]

Posthemorrhagic HC (PHH) occurs in 35% of PT/low-birth-weight patients with IVH, and approximately 15% of those with PHH eventually require treatment with a VP shunt.[42] Acutely, HC occurs due to obstruction of the ventricular system or arachnoid villi by red blood cells and their breakdown products. Arachnoidal reaction, most prominent in the cisterna magna, gradually progresses, resulting in an adhesive arachnoiditis that leads to subacute/chronic HC.[6,44] Poor neurodevelopmental outcomes are common in infants with IVH and PHH (especially chronic HC) and include seizures, motor handicaps, cognitive delay, and visual impairment.[42] White matter injury (eg, PVL) may be associated with ventriculomegaly due to *ex vacuo* dilatation. It may be difficult to distinguish ventriculomegaly due to PVL from that associated with PHH, and they may coexist.

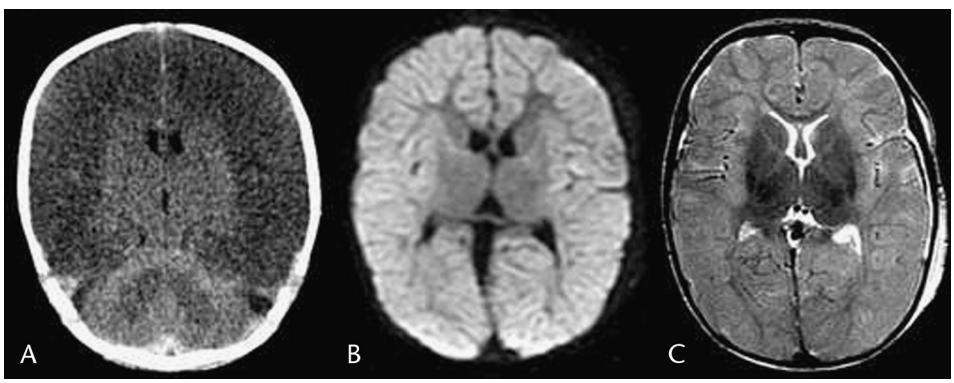

FIGURE 6. Hypoxic-ischemic injury in a 25-day-old girl. A, Noncontrast CT at presentation shows diffuse cerebral hemispheric hypodensity with loss of gray-white differentiation and less involvement of the basal ganglia, thalami, and cerebellum (white cerebellum sign). Cerebral swelling is associated with effacement of the sulci and ventricles. Magnetic resonance imaging was done the next day. B, Axial DWI shows diffuse high-intensity, restricted diffusion throughout the cerebral cortex (confirmed by apparent diffusion coefficient map). C, Axial T2 image shows diffusely increased intensity of the cerebral cortex with effacement of fissures and sulci.

© 2007 Lippincott Williams & Wilkins

Copyright © Lippincott Williams & Wilkins. Unauthorized reproduction of this article is prohibited.

TABLE 3. Causes of HC in Infancy and Childhood

Developmental	Acquired
Chiari II malformation	Posthemorrhage
Aqueductal anomalies	Postinfection
Congenital cysts/DW malformation	Posterior fossa tumors
Encephalocele	Tumors about the third ventricle
Hydranencephaly	Cerebral hemispheric tumors
Craniosynostosis	
Skull base anomalies	
Foraminal atresia	
Immature arachnoid villi	
Vein of Galen aneurysm	

T2/fluid-attenuated inversion recovery (FLAIR) periventricular white matter hyperintensity, loss of the periventricular white matter volume, and irregular ventricular margins are findings characteristic of PVL (Fig. 15).[45–47]

Subarachnoid and intraventricular hemorrhage in full-term infants is less common than in PT infants and may be due to coagulopathy, dehydration, hypoxic-ischemic injury, venous thrombosis, infection, or trauma (including birth-related trauma) (Fig. 16).[48] Although the mechanism of acute and chronic PHH is similar to that for PT infant, outcome is more variable for the term infant.[6]

Venous hypertension due to venous thrombosis should be considered in infants presenting with unexplained seizures and irritability or in those with hemorrhage or infarct not corresponding to an arterial vascular territory. Venous hypertension may be due to developmental conditions such as

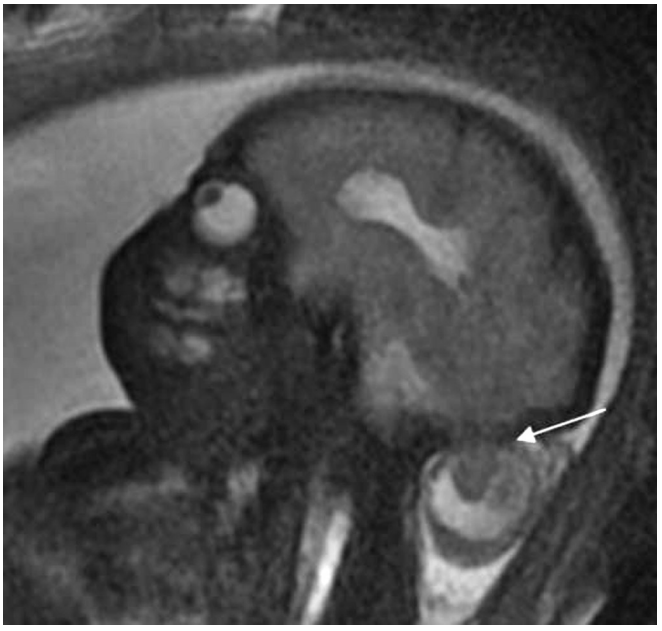

FIGURE 7. Occipital encephalocystocele in 28-week-old fetus. Sagittal T2–single-shot fast spin echo image shows herniation of dysplastic occipital lobe, dura, and CSF through a small occipital defect (white arrow) with associated ventriculomegaly.

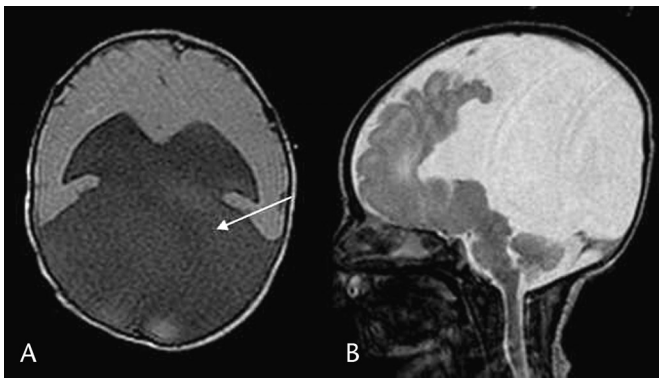

FIGURE 8. Holoprosencephaly in a 5-day-old baby. Axial T1 (A) and midsagittal T2 (B) images show a large monoventricle with large dorsal cyst (white arrow) along with a partial anterior interhemispheric fissure, absent corpus callosum, and small posterior fossa.

malformations of the skull base restricting venous outflow (eg, achondroplasia) or congenital heart disease or pulmonary disease with elevated central venous pressures. It may be acquired due to thrombosis of cerebral veins or sinuses from various causes such as infection, vascular malformation, or coagulopathy (Fig. 17). In an evaluation of suspected venous thrombosis, Doppler US, contrast-enhanced CT, computed tomographic angiography, MRI with MR venogram and gadolinium enhancement, or catheter angiography may be needed to directly demonstrate dural venous sinus thrombosis. Cortical, subependymal, or medullary venous occlusion may not be directly demonstrated by these techniques, although hemorrhages or thromboses may be present in those distributions. The thrombosis may appear as computed tomographic hyperdensity, T1 high-intensity, T2 low-intensity, or GRE hypointensity and can mimic hemorrhage. Intravenous enhancement about the thrombus may be seen as an empty "δ" sign. Depending upon the clinical context, treatment may be directed only to the specific cause (eg, infection) or may

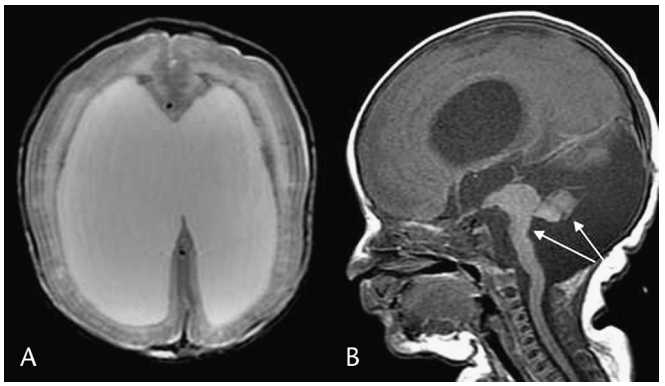

FIGURE 9. Walker-Warburg syndrome in a 2-day-old girl. Axial T2 (A) and sagittal T1 (B) images show marked third and lateral ventriculomegaly with absent septum pellucidum and callosal hypogenesis. There is cortical mantle thinning with an irregular gyral pattern (cobblestone lissencephaly), hypogenesis of the pons and cerebellar vermis (white arrows), and tectal dysplasia with aqueductal stenosis.

© 2007 Lippincott Williams & Wilkins

Copyright © Lippincott Williams & Wilkins. Unauthorized reproduction of this article is prohibited.

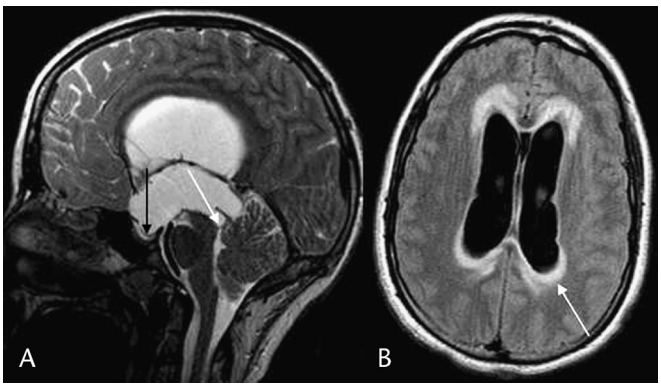

FIGURE 10. Hydrocephalus due to aqueductal stenosis. A, Sagittal T2 image demonstrates the aqueductal web (white arrow), small fourth ventricle, and marked third ventricular enlargement with ballooning of the anterior and posterior recesses plus downward displacement of the floor into the sella (black arrow). B, Axial FLAIR image shows the markedly dilated lateral ventricles with hyperintense periventricular edema (white arrow).

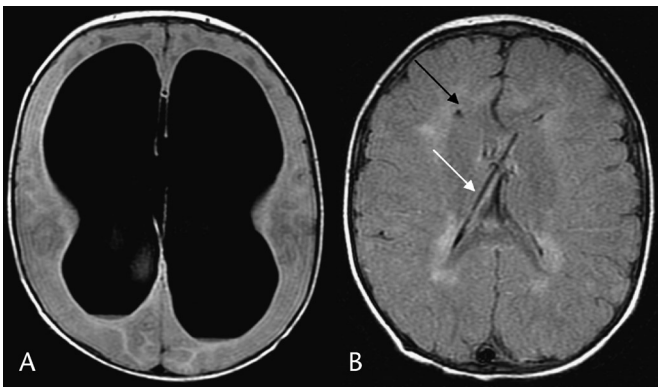

FIGURE 12. Communicating HC post-VP shunt in a 4-year-old boy. A, Axial FLAIR image at presentation in early infancy demonstrates marked ventriculomegaly with thinning of the cortical mantle. B, Follow-up axial FLAIR image shows a right parietal ventricular catheter in place (white arrow), small ventricles, and increased mantle thickness. The periventricular white matter hyperintensity (black arrow) likely represents undermyelination vs some leukomalacia or gliosis.

also include anticoagulation or thrombolysis.[49–53] Increased pressure within the dural sinuses creates a decreased pressure gradient across the arachnoid villi that results in decreased CSF resorption. In the setting of venous hypertension, either HC or pseudotumor cerebri may occur depending on patient age and patency of the cranial sutures. In young infants (less than 18 months) who have open sutures, an expansile calvarium, and soft, undermyelinated, immature white matter, HC is more likely to occur because the ventricles may expand without resistance. Pseudotumor is more common in older infants and children.[6]

Postinfectious HC

Hydrocephalus in infants may be the result of prenatal or postnatal infection. Prenatal infections occur either by ascending infection from the cervix to the amniotic fluid (usually bacteria or herpes) or via hematogenous dissemination through the placenta (eg, toxoplasmosis, other infections, rubella, cytomegalovirus [CMV] infection, and herpes simplex infections and other viruses). During the first 2 trimesters, infection will typically lead to malformations. In the third trimester, destructive lesions occur. Ventriculomegaly is often due to cerebral destruction, but HC may also occur and is most ommon in toxoplasmosis. A comprehensive review of prenatal infections is described elsewhere. Features of the 2 most common entities (CMV and toxoplasmosis) are described below.[6,11,53]

Congenital CMV infection is a common and serious viral infection among newborns. Depending on the timing of the insult, signs and symptoms include hepatosplenomegaly, microcephaly, chorioretinitis, and seizures.[6,53] Affected patients have varying degrees of lissencephaly/polymicrogyria, decreased cerebral white matter, astrogliosis, cerebral calcification, delayed myelination, and cerebellar hypoplasia.[54,55] Ventriculomegaly is usually related to cerebral underdevelopment/destruction, rather than HC (Fig. 18). Infection during early gestation tends to result in more severe

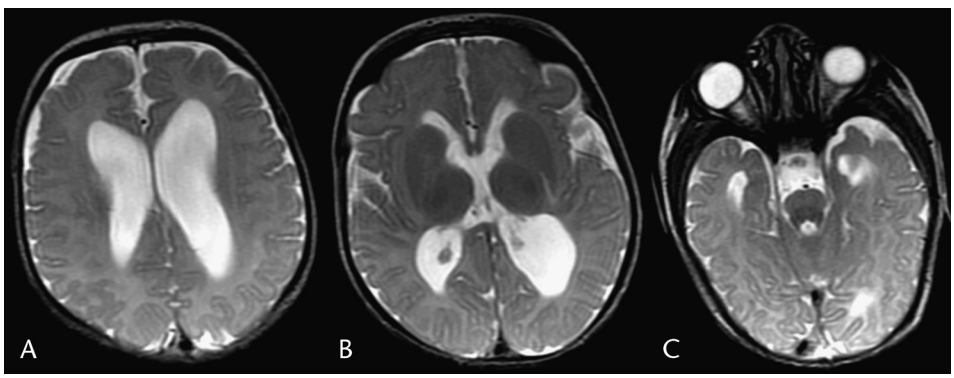

FIGURE 11. Cerebral underdevelopment in an infant with tetralogy of Fallot. Axial T2 images (A–C) show lateral ventricular enlargement out of proportion to the third ventricle and temporal horns. The sylvian fissures are wide. Normal hyperintensity is seen within the cerebral white matter due to immaturity. The findings suggest underdevelopment, rather than HC, although a component of communicating HC is always difficult to exclude and may coexist with any cause of underdevelopment or atrophy.

© 2007 Lippincott Williams & Wilkins

Copyright © Lippincott Williams & Wilkins. Unauthorized reproduction of this article is prohibited.

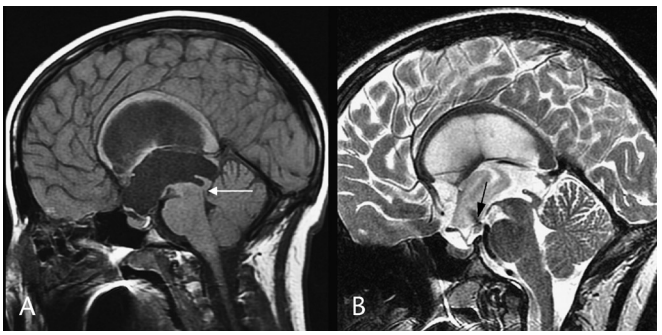

FIGURE 13. Endoscopic third ventriculostomy. A, Sagittal T1 image shows aqueductal stenosis (white arrow) with third and lateral ventricular enlargement. B, Post-ETV sagittal T2 image shows a CSF flow void across the ETV (black arrow) along with decreased enlargement of the third ventricular and less ballooning of the anterior recesses.

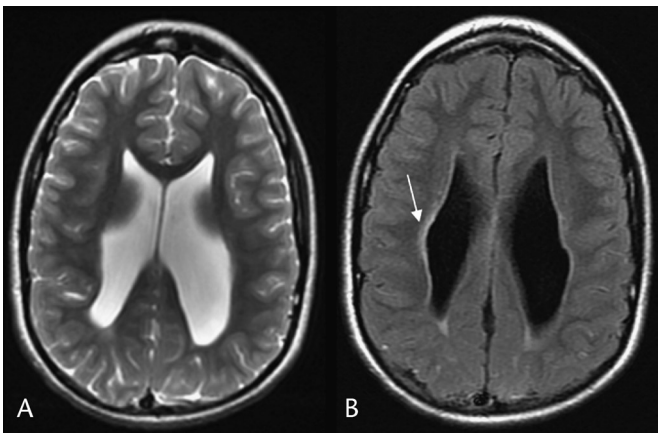

FIGURE 15. Periventricular leukomalacia. Axial T2 (A) and axial FLAIR (B) images show lateral ventriculomegaly with irregular margins, periventricular high intensities (white arrow), and decreased white matter volume.

disease. Computed tomography often detects cerebral calcifications (eg, periventricular). Magnetic resonance imaging best demonstrates the parenchymal involvement.[11,54,55] Congenital toxoplasmosis may manifest at birth or days to weeks later. There may be generalized or predominantly CNS involvement. Calcifications are common and more random in distribution, including periventricular, cortical, and basal ganglia. Hydrocephalus often results from the granulomatous meningeal or ependymal reaction that can cause aqueductal stenosis and communicating HC. Ventriculomegaly may also occur secondary to cerebral tissue destruction. Malformations of cortical development (eg, polymicrogyria) are uncommon.[11,53,56]

Postnatal meningitis may be bacterial, viral, fungal, or parasitic and caused by direct (eg, sinus or ear infection) or hematogenous spread. Common etiologies include Gram-negative bacteria (eg, *Escherichia coli*), group B streptococcus, pneumococcus, *Listeria*, neisseria, and tuberculosis. In the acute-subacute setting, meningitis can lead to HC due to clumping of purulent fluid along the CSF pathways or due to inflammation of arachnoid granulations with reduced CSF resorption. Chronically, the presence of inflammatory exudate and blood products lead to arachnoiditis. Fungal and granulomatous meningitides are more likely to cause clinically significant HC than bacterial and viral infections. The severity of HC is also related to the duration and severity of infection.[56–59] Normal imaging evaluation does not exclude CNS infection. Magnetic resonance imaging may sometimes demonstrate meningeal enhancement. In fungal and granulomatous infection, the meningeal enhancement and thickening often has a predilection for the basal cisterns. Magnetic resonance imaging is mainly used to evaluate the sequelae and complications of meningitis. Arachnoid loculations due to arachnoid scarring may occur and simulate arachnoid cysts (ACs). Ventricular dilatation may be shown by MR or CT. Other complications of meningitis, including venous thrombosis, infarction (arterial or venous), ventriculitis, cerebritis, abscess, and subdural empyema, are best delineated with MRI (Fig. 19).[56,58,59]

DEVELOPMENTAL MALFORMATIONS

Chiari II

Chiari II malformation accounts for about one third of infantile HC. Almost all present at birth with a MMC.

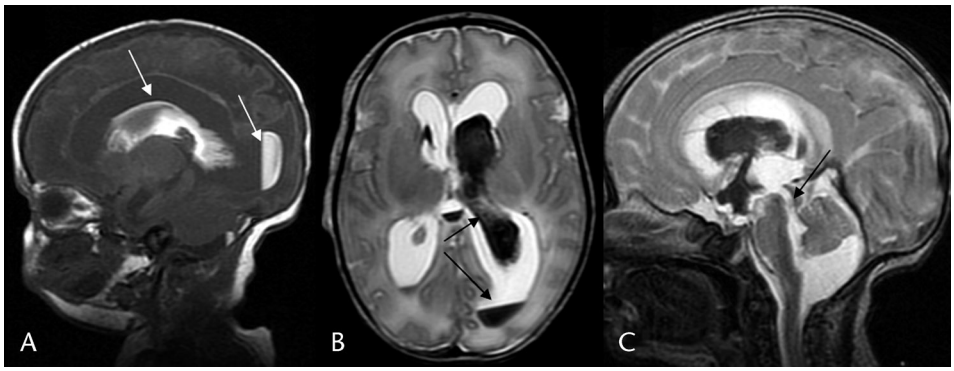

FIGURE 14. Preterm PHH. Sagittal T1 (A) and axial T2 (B) images shows moderate-to-marked ventriculomegaly with left subependymal and intraventricular hemorrhages (arrows) that are T1 hyperintense and T2 hypointense. Midsagittal T2 image (C) shows a widely patent aqueduct (black arrow) and large cisterna magna, consistent with communicating HC.

© 2007 Lippincott Williams & Wilkins

Copyright © Lippincott Williams & Wilkins. Unauthorized reproduction of this article is prohibited.

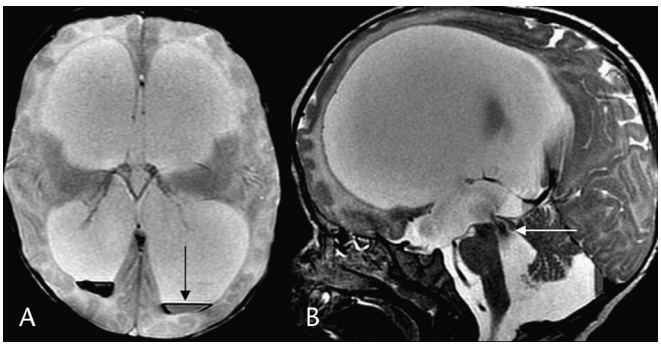

FIGURE 16. Nonpreterm, posthemorrhagic communicating HC. Axial GRE (A) and midsagittal T2 (B) images demonstrate marked lateral, third, and fourth ventriculomegaly with ill-defined ventricular margins, CSF-blood levels (black arrow), and a prominent flow-void within the patent aqueduct (white arrow), consistent with communicating HC.

Hydrocephalus usually develops after repair of the MMC. Altered CSF flow likely results from the abnormal low position of the fourth ventricular exit foramina below the foramen magnum, causing poor connection between the spinal and intracranial subarachnoid spaces. Hydrocephalus manifests when the surgically closed MMC no longer acts as a pressure valve to release CSF that flows freely from the ventricles into the central canal.[21,60] Chiari II malformation results from failure of neural tube closure, The cerebellar vermis herniates into the cervical spinal canal and may degenerate. The fourth ventricle is low, vertically oriented, and narrowed. The pons is stretched inferiorly and is also narrowed. The medulla may extend below foramen magnum and a cervicomedullary kink may be seen. The tectum has a beaked or blunted shape. Petroclival scalloping may be seen along with persistent or accentuated Luckenshadl (ie, lacunar skull).[21,60–63] Other commonly associated anomalies include hypogenesis of the corpus callosum, heterotopias, colpocephaly, and polygyria or stenogyria (Fig. 20).[6,60–62] The fourth ventricle may herniate behind the medulla and below the vermis (ie, "encysted"). More importantly, it may become isolated or trapped due to poor inflow (eg, primary aqueductal stenosis or secondary closure from shunting) and poor outflow (exit foraminal atresia or closure). A normal-sized or large fourth ventricle in Chiari II patients may indicate trapping or shunt malfunction. Increasing hydrosyringomyelia may also result from worsening HC, shunt malfunction, or fourth ventricular isolation.[63] After shunting, the medial walls of the ventricular trigones may appear deformed by a large CSF-containing structure. This results from "mantle collapse" of the dysplastic adjacent cortex and should be differentiated from an AC or atrial diverticulum.[6] Hydrocephalus (or hydrosyringomyelia) may also be seen with other Chiari malformations (eg, I, III).

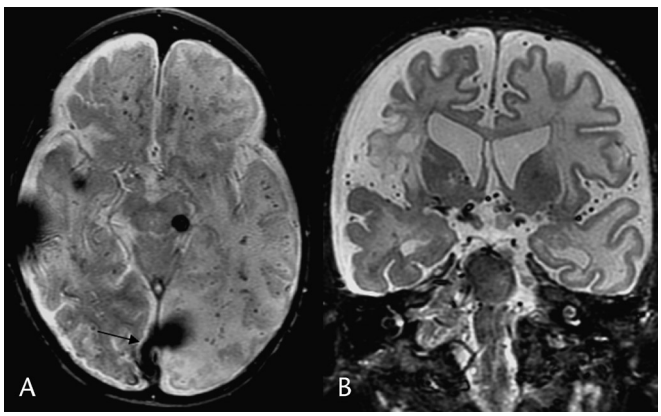

FIGURE 17. Chronic venous hypertension due to dural arteriovenous fistula and extensive venous thrombosis. Axial GRE (A) and coronal T2 (B) mages show partially thrombosed and dilated torcula (black arrow), cerebral white matter hyperintensity secondary to venous congestion and chronic ischemia, numerous tiny foci of hypointensity due to hemorrhage and/or thromboses, ventriculomegaly, and large subarachnoid spaces.

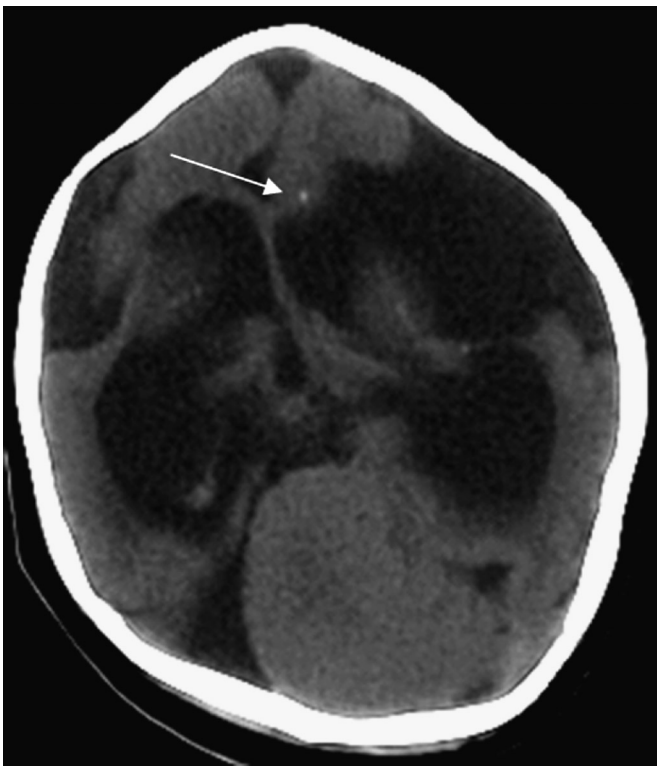

FIGURE 18. Congenital CMV. Noncontrast CT demonstrates ventriculomegaly with bilateral porencephaly, periventricular calcifications (white arrow), and dysplastic cerebellum.

Dandy Walker Blake Continuum

Posterior fossa cystic malformations may be categorized along a continuum, including the Dandy-Walker malformation (DWM), Dandy-Walker variant (DWV), mega cisterna magna (MCM), and Blake pouch cyst (BPC) or retrocerebellar AC (RCAC). The classic Dandy-Walker malformation is characterized by complete or partial vermian agenesis (especially inferior vermis), a large retrocerebellar cyst (ie, "combined fourth ventricle and cisterna magna"),

© 2007 Lippincott Williams & Wilkins

Copyright © Lippincott Williams & Wilkins. Unauthorized reproduction of this article is prohibited.

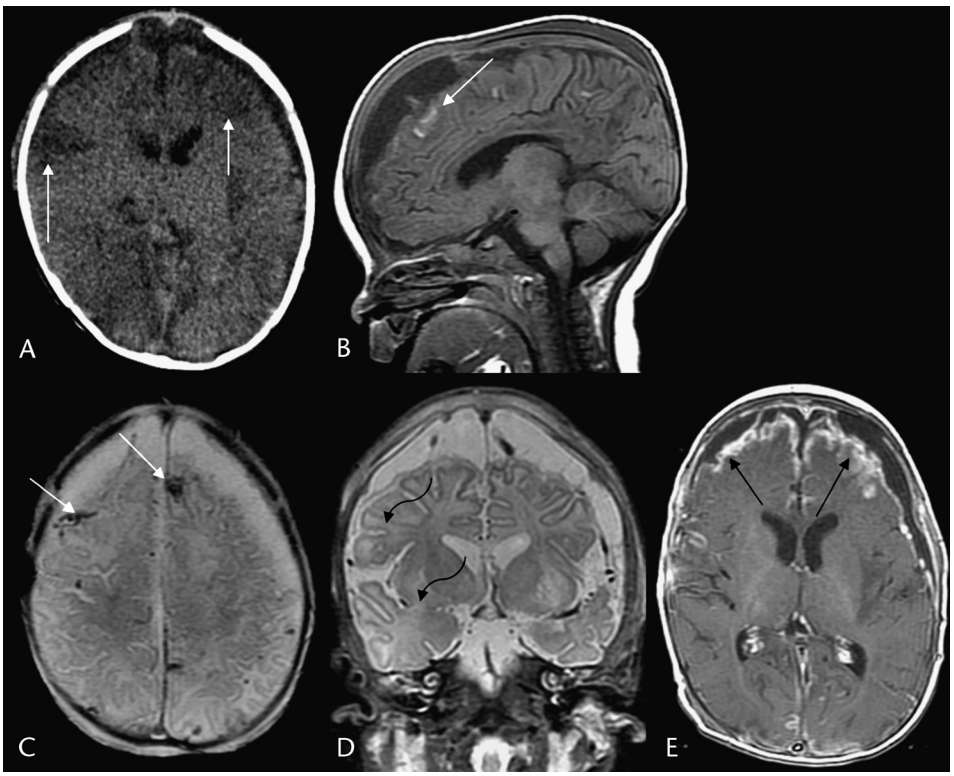

FIGURE 19. Pneumococcal meningitis in a 2-month-old boy. A, Noncontrast CT demonstrates multiple cortical and white matter hypodensities (white arrows) consistent with edema, cerebritis, or multifocal infarctions. Hyperdensities are consistent with hemorrhage or thromboses. The asymmetric extracerebral low densities likely represent subdural collections. Magnetic resonance imaging was done 1 week later. Sagittal T1 (B), axial GRE (C), coronal T2 (D), and axial postgadolinium T1 (E) images show T1-hypointense/T2-hyperintense extracerebral collections that are DWI hypointense (not shown). These likely represent subdural effusions, rather than empyemas. In addition, there is mild ventriculomegaly. Bilateral linear and nodular cerebral and extracerebral foci that are T1 hyperintense and T2/GRE hypointense (white arrows) represent hemorrhages or thromboses. Multifocal cerebral white matter and basal ganglia T2 hyperintensities likely represent edema or infarctions (curved arrows), and some show enhancement. Thick, irregular, leptomeningeal enhancement is seen over the convexities (black arrows) and along the basal cisterms.

an enlarged posterior fossa, elevation of the torcular above the λ, and absence of the falx cerebelli. Associated CNS and systemic anomalies are common, including corpus callosum hypogenesis, polymicrogyria, heterotopias, cephalocele, and holoprosencephaly (Fig. 21). Hydrocephalus occurs in most patients but usually does not develop until after the neonatal

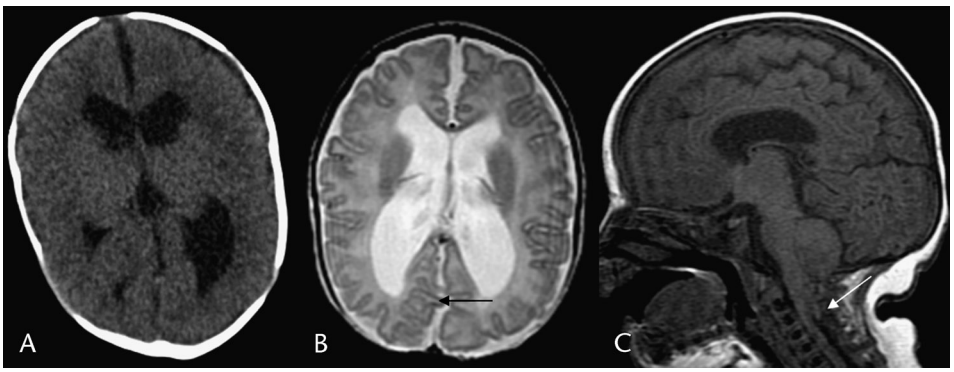

FIGURE 20. Chiari II in a 12-day-old boy. Axial CT (A) shows dysmorphic and enlarged lateral ventricles (a large foramen magnum with no fourth ventricle was also observed along with other characteristic findings—see text). Sagittal T1 (B) and axial T2 (C) images show a small posterior fossa, low tentorium, and herniation of the cerebellar vermis into the cervical canal posterior to a low cervicomedullary junction (white arrow). The fourth ventricle is elongated and small. Tectal beaking is present along with occipital polygyria/stenogyria (black arrow). Moderate to marked third and lateral ventriculomegaly is present with disproportionate enlargement of the posterior horns.

© 2007 Lippincott Williams & Wilkins

Copyright © Lippincott Williams & Wilkins. Unauthorized reproduction of this article is prohibited.

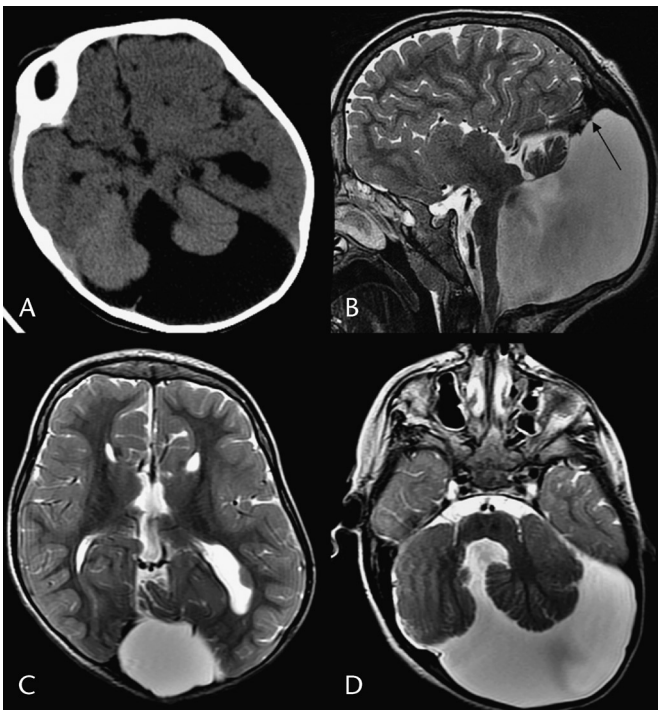

FIGURE 21. Dandy-Walker malformation. Noncontrast CT (A) plus sagittal (B) and axial (C–D) MRI images show an enlarged posterior fossa with elevated torcula (black arrow), cerebellar vermis hypogenesis, and a retrocerebellar cyst that communicates with the fourth ventricle. Agenesis of the corpus callosum and lateral ventricular dysmorphia is also shown.

period. Evaluation of aqueductal patency is important before surgery for ventricular or cyst shunting.[22,64–66] In DWV, the cerebellar vermis is hypogenetic, the posterior fossa is usually of normal size, and there is separation of the fourth ventricle from a smaller retrocerebellar "cyst." If the cerebellar vermis is completely formed and an enlarged retrocerebellar CSF space is present, the anomaly is usually designated MCM. An associated wide vallecula (increased medullary-vermian angle) suggests BPC. If the retrocerebellar CSF collection exerts mass effect on a completely formed cerebellum, then RCAC may be diagnosed, especially if there is HC. Other CNS or systemic anomalies are uncommon in DWV, MCM, BPC, or RCAC. These "cystic" posterior fossa anomalies are

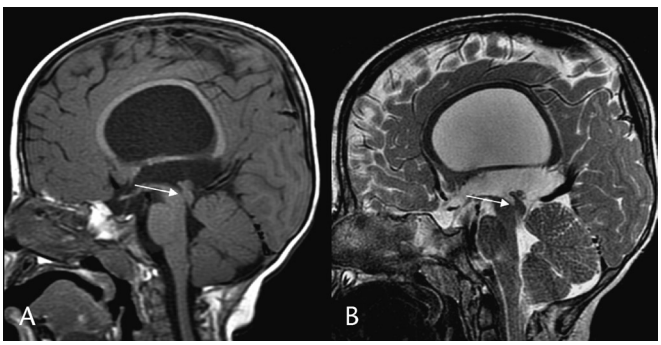

FIGURE 22. Aqueductal stenosis. Sagittal T1 (A) and T2 (B) images show enlarged third and lateral ventricles (thinning of the corpus callosum) with normal fourth ventricle. Focal discontinuity of the cerebral aqueduct is seen (white arrows), and there is absence of the usual CSF flow void. The tectum may be dysmorphic, but no mass is present. The thin-section sagittal T2 image is especially helpful for delineating anatomy of the third ventricle and basilar cisterns in anticipation of ETV.

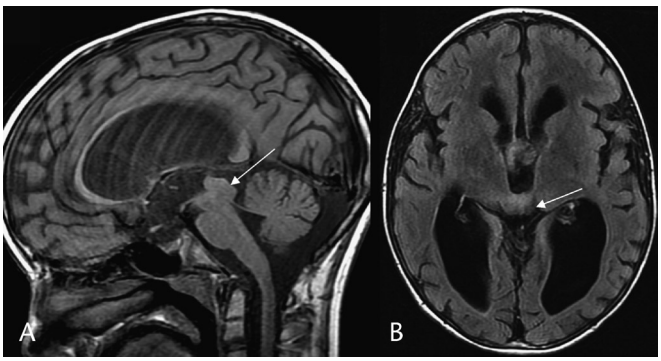

FIGURE 23. Tectal glioma. Sagittal T1 image (A) shows third and lateral ventriculomegaly with a tectal mass (white arrow) and aqueductal narrowing. Axial FLAIR image (B) shows the hyperintense tectal mass (white arrow). There was minimal gadolinium enhancement (not shown). Hyperintense FLAIR CSF flow artifact is present in the anterior third ventricle.

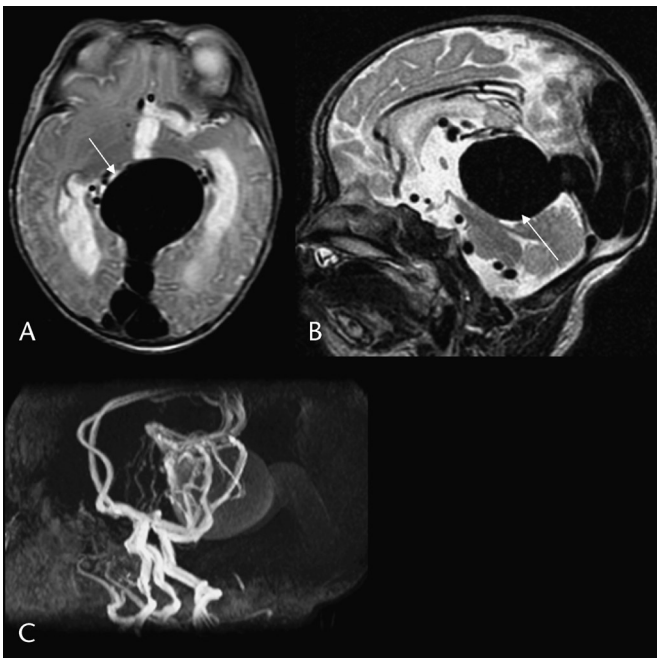

FIGURE 24. Vein of Galen malformation, choroidal type. Axial (A) and sagittal (B) T2 images show an enlarged vein of Galen (promesencephalic vein) (white arrows) with dilated straight sinus and superior sagittal sinus flow voids plus adjacent arterial feeder flow voids. Lateral and third ventriculomegaly represents HC (aqueduct compression vs venous hypertension). Lateral reprojected time of flight–MR angiography image (C) shows the high-intensity flow features of the multiple arteriovenous fistulae.

© 2007 Lippincott Williams & Wilkins

Copyright © Lippincott Williams & Wilkins. Unauthorized reproduction of this article is prohibited.

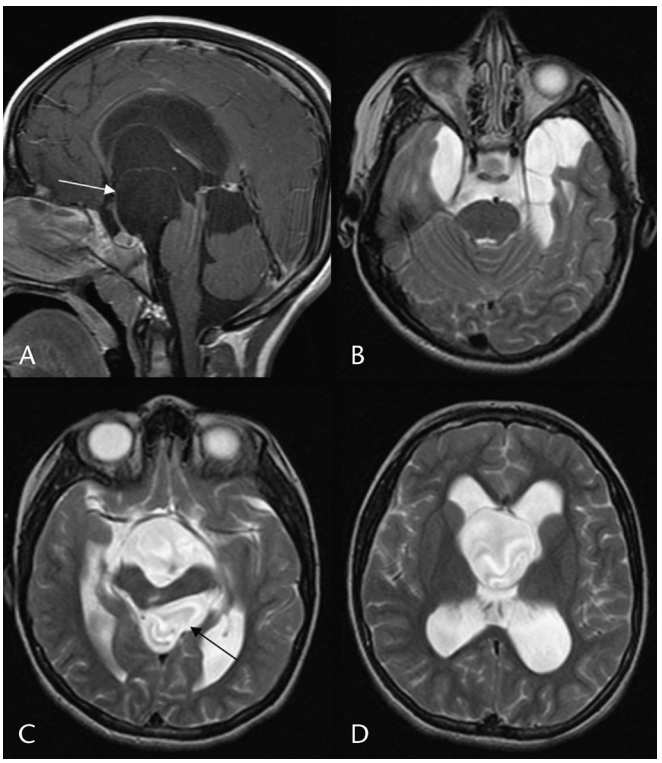

FIGURE 25. Multiple arachnoid cysts. A, Sagittal T1 (A) and axial T2 (B–D) images show a large, CSF-intensity suprasellar/prepontine cyst (white arrow) that deforms the adjacent pituitary stalk, elevates the dilated third ventricle, and extends to the foramina of Monro. A smaller quadrigeminal plate cyst (black arrow) deforms the adjacent tectum, aqueduct, and superior vermis. There are associated bilateral middle cranial fossa cysts and HC with marked third and lateral ventriculomegaly.

to be distinguished from cerebellar hypoplasia (formed but small cerebellum without cyst), pontocerebellar hypoplasia (formed but small pons and cerebellum), Joubert syndrome (superior or total vermian hypogenesis), rhombencephalosynapsis (absent vermis with fused hemispheres), and cerebellar atrophy or degeneration (small cerebellum with prominent fissures).[22,64–66]

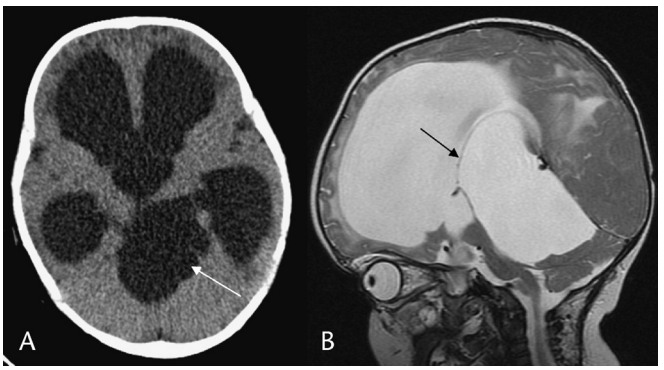

FIGURE 27. Supracerebellar AC in a 7-month-old boy. Noncontrast CT (A) shows a well-defined CSF-density mass in the upper posterior fossa (white arrow) and marked third and lateral ventriculomegaly. Sagittal T2 image (B) shows the large cyst (black arrow) that displaces/compresses the cerebellar vermis and fourth ventricle inferiorly, and the brain stem and aqueduct anteriorly. It extends through the tentorial hiatus, displaces the straight sinus superiorly, and compresses the posterior third ventricle.

Aqueductal Stenosis

Aqueductal narrowing may be primary (ie, maldevelopmental) or secondary (ie, acquired, eg, adhesive ependymitis). It is a common cause of HC and may be isolated or associated with other developmental or acquired conditions. Developmental narrowing may be in the form of stenosis, gliosis, forking (ie, fenestration), or a membrane (ie, aqueductal web). Hemorrhage, infection, or tumors may lead to acquired aqueductal stenosis. Onset of symptoms due to primary aqueductal stenosis is insidious and may occur any time from birth to adulthood.[67] Computed tomography often shows dilatation of the third and lateral ventricles with normal or small fourth ventricle. There may be tectal dysplasia with thickening or beaking. This is to be distinguished from a tectal glioma. The latter may not be apparent on CT.

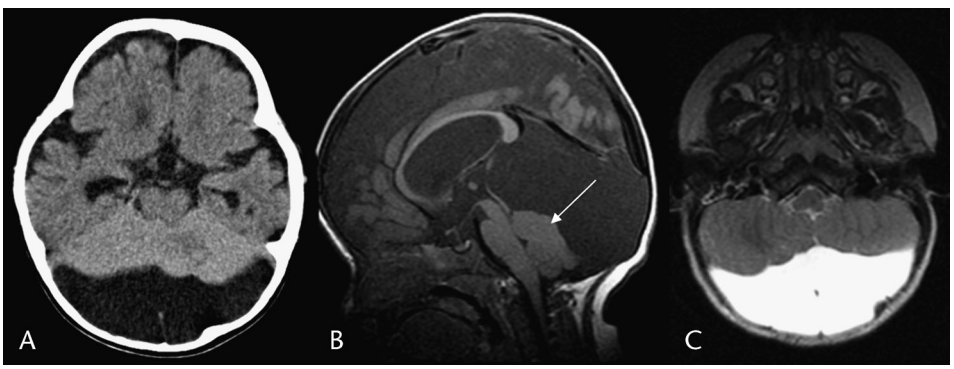

FIGURE 26. Retrocerebellar arachnoid cyst. Noncontrast CT (A) shows the low-density CSF collection behind the deformed cerebellum along with dilated temporal horns. Sagittal T1 (B) and axial T2 (C) images show a large cyst that expands the posterior fossa and compresses the formed vermis (white arrow) and cerebellar hemispheres. The fourth ventricle and aqueduct are open but compressed, resulting in HC.

© 2007 Lippincott Williams & Wilkins

Copyright © Lippincott Williams & Wilkins. Unauthorized reproduction of this article is prohibited.

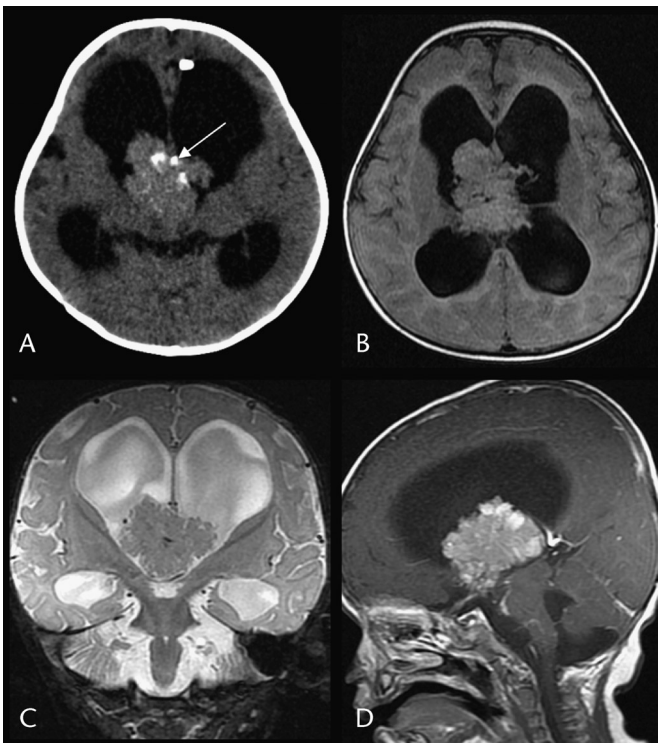

FIGURE 28. Choroid plexus papilloma in a 7-month-old girl. Noncontrast CT (A) shows a midline intraventricular mass with calcifications (arrow), enlarged ventricles, and a portion of the left frontal ventricular catheter. Axial T1 (B), coronal short τ inversion recovery (C), and sagittal postgadolinium T1 (D) images show the lobulated third ventricular mass that is isointense and markedly enhancing. There is extension through the foramina of Monro and marked lateral ventriculomegaly.

Magnetic resonance imaging is always indicated. Sagittal T1 and T2 images demonstrate the level of aqueductal stenosis and absence of a CSF flow void (Fig. 22). T2 and FLAIR images detect tectal- and pineal-region lesions (Fig. 23). Gadolinium T1 images may show enhancement, although tectal gliomas enhance less often than pineal region germ cell tumors (GCTs) or pineoblastomas.[67–70]

MASSES

Most masses of infancy are cystic or cyst-like and include the Dandy-Walker-Blake spectrum, arachnoid or glioependymal cysts (retrocerebellar, suprasellar, intraventricular, quadrigeminal plate cistern), porencephaly, encephalocele, and the vein of Galen malformation (varix) as a blood-filled cyst (Fig. 24). Neoplasm as an expanding mass or an obstructive lesion is a rare cause of ICP or HC in infancy.[9,17,18] Beyond infancy, neoplasm becomes the leading consideration.

Arachnoid Cysts

Arachnoid cysts of maldevelopmental origin are congenital lesions composed of an arachnoid membrane that secretes CSF to expand the cyst. Acquired ACs (eg, leptomeningeal cysts or arachnoid loculations) are loculations of CSF that are associated with arachnoid scarring. The most common locations for AC are the Sylvian fissures followed by the suprasellar cistern (Fig. 25), quadrigeminal cistern, cerebellopontine angle, and retrocerebellar space (Fig. 26). Less common sites for AC include the interhemispheric fissures, cerebral convexities, and anterior midline portion of the posterior fossa (Fig. 27). Congenital ACs are usually sporadic but occur with increased incidence in patients with autosomal dominant polycystic kidney disease.[6,71] Arachnoid cysts are often incidental findings on imaging for other indications. However, mechanical effects may result in headaches, seizures, ICP, or HC. Suprasellar AC is to be distinguished from other cystic lesions in this region, including Rathke cyst, craniopharyngioma, dermoid-epidermoid, teratoma, and cystic astrocytomas. Large ACs in this location displace the third ventricle superiorly and may obstruct the lateral ventricles at the foramina of Monro. Quadrigeminal plate ACs may displace the pineal gland and occlude the aqueduct. Posterior fossa ACs were described earlier. Middle cranial fossa cysts may become very large and can cause mass effect with expansion of the hemicranium.

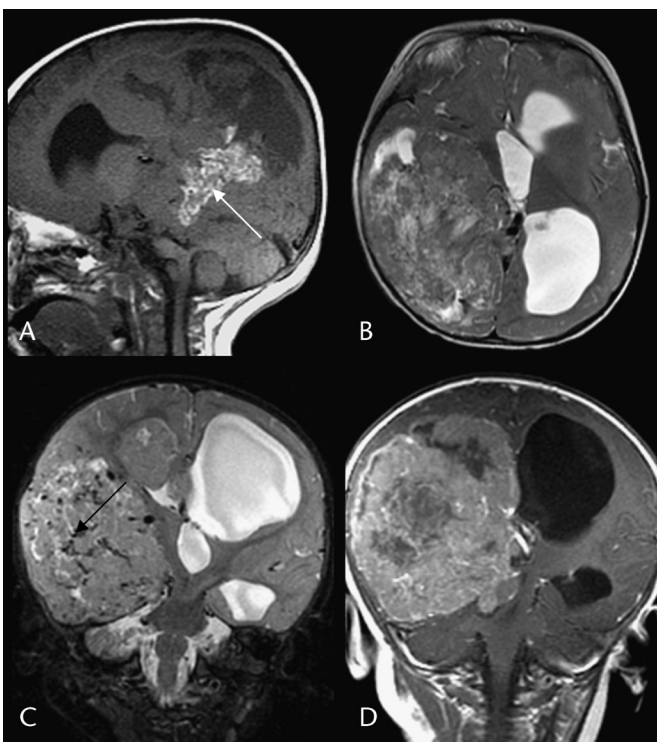

FIGURE 29. Choroid plexus carcinoma. Sagittal T1 (A), axial and coronal T2 (B–C), and coronal postgadolinium T1 (D) images show a heterogeneous mass within the right lateral ventricle. Hypervascularity, with numerous flow voids (black arrow), is seen along with calcifications, hemorrhage (white arrow), and marked enhancement. The mass extends into the adjacent cerebrum, and there is marked ventriculomegaly. Similar imaging features may be seen with periventricular PNET, ependymoma, or ATRT and intraventricular extension.

© 2007 Lippincott Williams & Wilkins

Copyright © Lippincott Williams & Wilkins. Unauthorized reproduction of this article is prohibited.

FIGURE 30. Choroid plexus papilloma postresection. A, Immediate postoperative noncontrast CT shows bifrontal craniotomy, large extracerebral air and fluid collections, a small amount of intraventricular hemorrhage, and moderately large lateral ventricles. A right frontal catheter (white arrow) is in place at the site of continuity between the extracerebral space and ventricular system. Noncontrast CT (B) 1 month after surgery shows smaller ventricles but larger extracerebral collections. The ventricular catheter was then replaced with an extracerebral (subdural) catheter.

These cysts may also be associated with subdural and intracystic hemorrhage, or subdural hygroma. This may occur spontaneously, after trauma, or after surgical fenestration.[6,72–74] On imaging, ACs are thin-walled, well-defined, cystic lesions that conform to CSF on all modalities. Ultrasonography shows a hypoechoic lesion with through transmission. On CT, a hypodense, nonenhancing lesion is seen with a defined wall. On MRI, the lesion follows CSF intensity on all sequences. Fluid-attenuated inversion recovery and diffusion-weighted imaging (DWI) differentiate AC (hypointensity) from epidermoid (high intensity), which may have a similar appearance on other sequences.[71,75]

Neoplasms

Neoplasms rarely occurring in the first 2 years of life include some astrocytomas, choroid plexus tumors, GCTs, embryonal tumors (ie, primitive neuroectodermal tumors [PNET]), and mesenchymal neoplasms (eg, atypical teratoid rhabdoid tumor [ATRT]).[9] Tumors in children have a predilection for the midline along the ventricular pathways and are often associated with ICP and HC. This includes the posterior fossa along the fourth ventricle and aqueduct (eg, medulloblastoma, astrocytoma, ependymoma, ATRT) and the supratentorial compartment about the third ventricle (eg, craniopharyngioma, astrocytoma, GCTs, PNET).[9,17] Deep cerebral tumors and cerebral hemispheric tumors (eg, astrocytoma, ependymoma, choroids plexus tumors, PNET, ATRT) may produce ICP or HC by mass effect and intracranial shift or present with seizures, hemiparesis, or other focal neurological deficits.

Supratentorial Intraventricular and Cerebral Hemispheric Tumors

The most common intraventricular tumors in early childhood are choroid plexus tumors. Choroid plexus tumors arise from epithelial cells of the choroid plexus and cause HC by either CSF overproduction or by CSF pathway obstruction due to mass effect or associated hemorrhage or seeding. Choroid plexus tumors usually originate in the lateral ventricles (most commonly in the trigone) but can arise anywhere that choroid plexus normally is present, including within the third and fourth ventricles. Choroid plexus tumors can be divided into CPP and choroid plexus carcinomas (CPCs), which are differentiated on the basis of histology rather than by gross pathologic finding or imaging. The classic appearance of a CPP on CT is that of a lobulated, isodense/hyperdense intraventricular mass that expands the ventricle and enhances brightly and homogenously. On MRI, the lesions are T2 isointense/hyperintense, show marked enhancement, and may demonstrate flow voids due to hypervascularity (Fig. 28). Punctate foci of calcification or hemorrhage may be seen within these lesions, and rarely, they may be bilateral. Aggressive CPP and CPC tend to be heterogeneous, contain cysts and hemorrhage, and may invade though the ventricular wall into the adjacent brain inciting edema (Fig. 29).[9,76–78] Cerebrospinal fluid seeding may also occur. In these cases, it may be difficult to distinguish

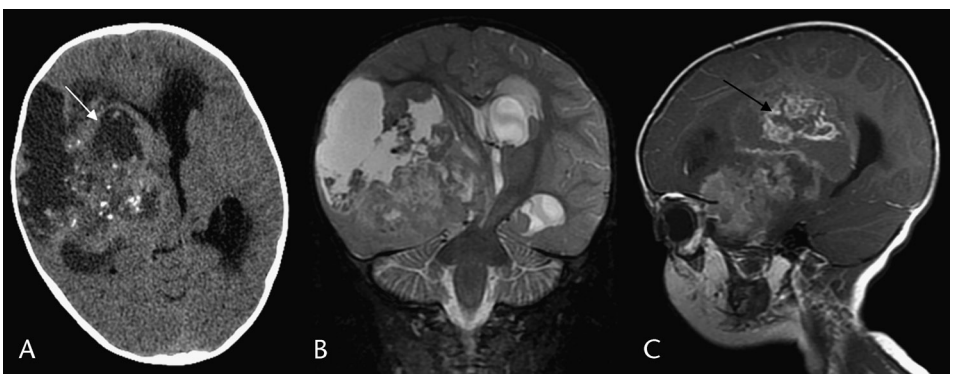

FIGURE 31. Cerebral ATRT in a 10-month-old boy. Noncontrast CT (A) shows a heterogeneous right hemispheric mass with calcification, cavitation (white arrow), and HC with periventricular edema. Coronal T2 (B) and sagittal postgadolinium T1(C) images show heterogeneous intensities and enhancement with cysts, necrosis, and mineralization (black arrow) plus mass effect, leftward shift, and HC with periventricular edema.

© 2007 Lippincott Williams & Wilkins

Copyright © Lippincott Williams & Wilkins. Unauthorized reproduction of this article is prohibited.

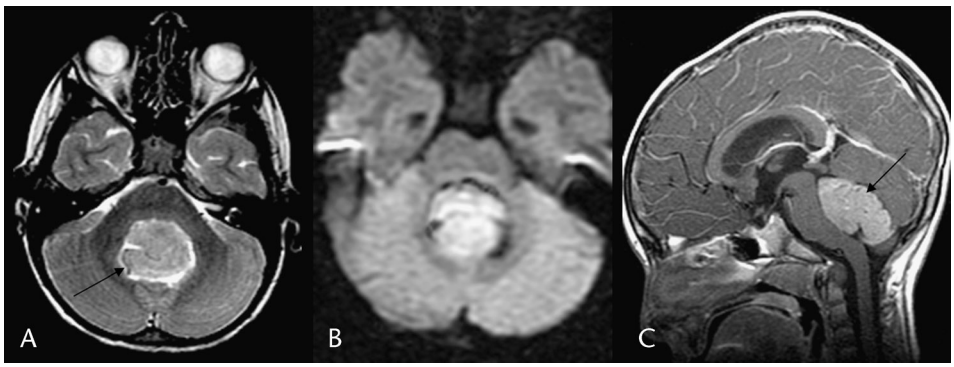

FIGURE 32. ''Typical'' medulloblastoma in a 5-year-old child. Axial T2 (A), DWI (B), and sagittal postgadolinium T1 (C) images show a midline posterior fossa mass (black arrows) growing into the fourth ventricle and associated with HC. The mass is T2 isohypointense to gray matter and CSF, DWI hyperintense (reduced diffusion), and markedly enhances.

CPC from periventricular PNET, ependymoma, or ATRT. Complete surgical resection of CPP results in a cure. However, the high vascularity of these tumors may prevent complete removal, especially for CPC. In addition, infants with complete tumor resection, whether CPP, CPC, or other large tumors, often require ongoing follow-up and management of the related HC, large extracerebral collections, and shunt malfunction (Fig. 30).[76,79,80] Rarely in infancy, a giant cell tumor or subependymal giant cell astrocytoma, associated with tuberous sclerosis, may arise at the foramen of Monro and produce asymmetric HC. Tumors of the cerebral hemispheres cause HC when lesions are large and cause herniation with compression of the lateral ventricles. Astrocytomas are the most common tumors of infancy and childhood and can range from pilocytic astrocytomas to glioblastoma multiforme. In infants, ATRT, ependymoma, PNET, and desmoplastic infantile tumors (gangliogliomas or astrocytomas) are other diagnostic considerations. Desmoplastic infantile tumors are low-grade cortical neoplasms that typically present with seizures. Atypical teratoid rhabdoid tumor and PNET are embryonal tumors and, similar to ependymoma, tend to have heterogeneous imaging features (Fig. 31).[6,9,76,81,85,89]

Posterior Fossa Tumors

Hydrocephalus commonly occurs with posterior fossa tumors. Tumor invasion, displacement, or compression results in obstruction at or below the level of the aqueduct and fourth ventricle. The most common posterior fossa tumors in infants and young children include medulloblastoma, ependymoma, ATRT, and astrocytomas (cerebellar and brain stem). Medulloblastomas are embryonal tumors that, in children, most commonly arise in the cerebellar vermis and grow into the fourth ventricle (Figs. 32, 33). The other typically midline lesion is ependymoma. Cerebrospinal fluid dissemination frequently occurs in medulloblastoma and may also occur in ependymoma (eg, anaplastic). Seeding may also cause communicating HC (Fig. 34). Medulloblastomas are cellular tumors that tend to be computed tomographic hyperdense, T2 isointense/hypointense, and markedly

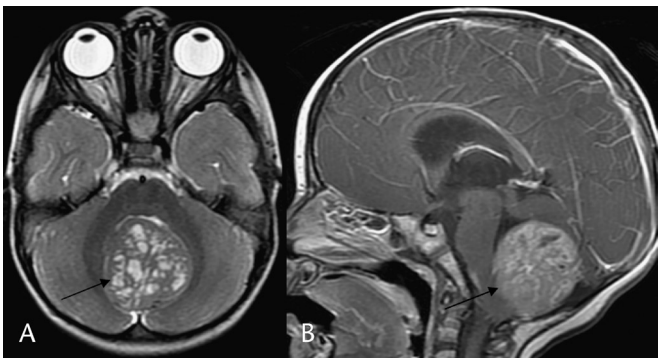

FIGURE 33. ''Atypical'' medulloblastoma in a 21-month-old child. Axial T2 (A) and sagittal gadolinium T1 (B) images shows a heterogeneously intense (multiple cavitations) and enhancing mass (black arrows) of the cerebellar vermis and fourth ventricle producing HC. Because of these imaging features and young age of the patient, the differential diagnosis also includes ependymoma, ATRT, and CPC.

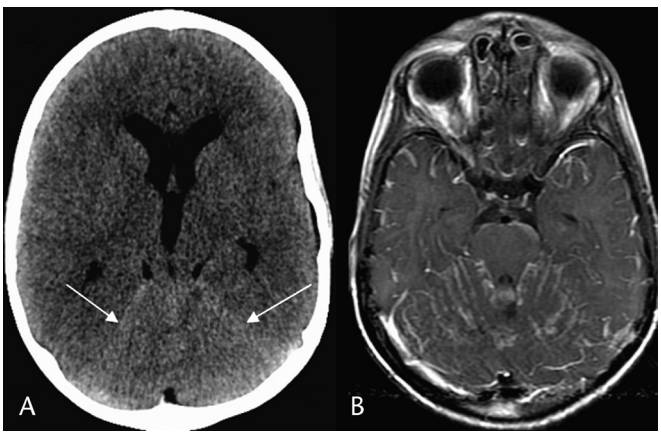

FIGURE 34. Medulloblastoma seeding with HC. Noncontrast CT (A) shows ventriculomegaly and accentuated high densities within the posterior fossa and along the tentorium (white arrows). Axial gadolinium T1 image (B) shows extensive leptomeningeal enhancement (seeding confirmed by lumbar puncture).

© 2007 Lippincott Williams & Wilkins

Copyright © Lippincott Williams & Wilkins. Unauthorized reproduction of this article is prohibited.

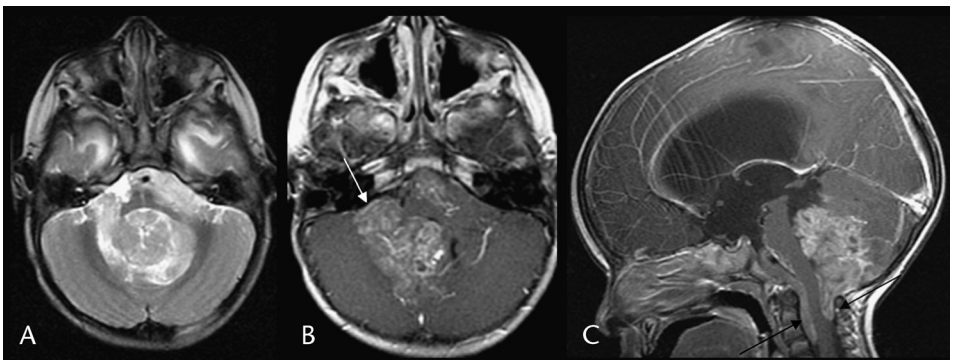

FIGURE 35. Ependymoma. Axial T2 (A) and axial (B) plus sagittal gadolinium T1 (C) images show a fourth ventricular mass that extends through the foramina of Luschka (white arrow) into both cerebellopontine angles and the prepontine cistern, as well as into the upper cervical canal about the medulla and cord (black arrows). There is marked HC. The mass exhibits heterogeneous intensity and enhancement. Atypical teratoid rhabdoid tumor and CPC may have a similar appearance.

enhances (Fig. 31). When atypical imaging features occur, the differential diagnosis should also include ependymoma, ATRT, and CPC (Fig. 32). Occasionally, a medulloblastoma that arises in the cerebellar hemisphere or has a major cystic component may mimic an astrocytoma. A fourth ventricular lesion that extends through the foramina of Luschka into the cerebellomedullary or cerebellopontine angle, or through foramen magnum into the cervical spinal canal, is characteristic of ependymoma (Fig. 35). Calcifications, cysts, and hemorrhage are more common than in other posterior fossa lesions and contribute to the heterogeneous density, intensity, and enhancement features of ependymoma. Atypical teratoid rhabdoid tumor may have a similar imaging appearance to medulloblastoma or ependymoma but has a different biologic behavior and a poorer prognosis.[81–86] Approximately 60% of astrocytomas in pediatric patients occur in the posterior fossa (2/3 cerebellum, 1/3 brain stem). Most cerebellar astrocytomas are juvenile pilocytic astrocytomas (JPAs). These are low-grade tumors that can often be totally excised and have excellent survival.[6] Juvenile pilocytic astrocytoma typically arises within the hemisphere and causes HC by mass effect. The classic appearance of JPA on CT and MRI is a cystic lesion with a brightly enhancing mural nodule (Fig. 36). However, some JPA may be cystic, solid, necrotic, or hemorrhagic. Brain stem astrocytomas may be focal or diffuse. Diffuse tumors smoothly expand the brainstem, have ill-defined margins, and rarely enhance and infrequently cause HC. Focal neoplasms are smaller, usually have well-defined margins or exophytic components, and often enhance and have a much better prognosis (likely due to resectability). Tectal gliomas tend to be low-grade lesions that cause HC even at small sizes (aqueductal stenosis) (Fig. 23). These lesions have a good prognosis and are usually managed with shunting or ETV and serial imaging.[6,9,69,81–83]

Tumors In and Around the Third Ventricle

Tumors in and around the third ventricle that cause HC include suprasellar lesions (chiasmatic, pituitary, and hypothalamic), thalamic lesions, and pineal region lesions. These lesions often obstruct CSF flow at the foramina of Monro, body of the third ventricle, and cerebral aqueduct, respectively. The most common neoplasms in the suprasellar region are chiasmatic-hypothalamic astrocytomas (pilocytic more than fibrillary). These may present with visual changes,

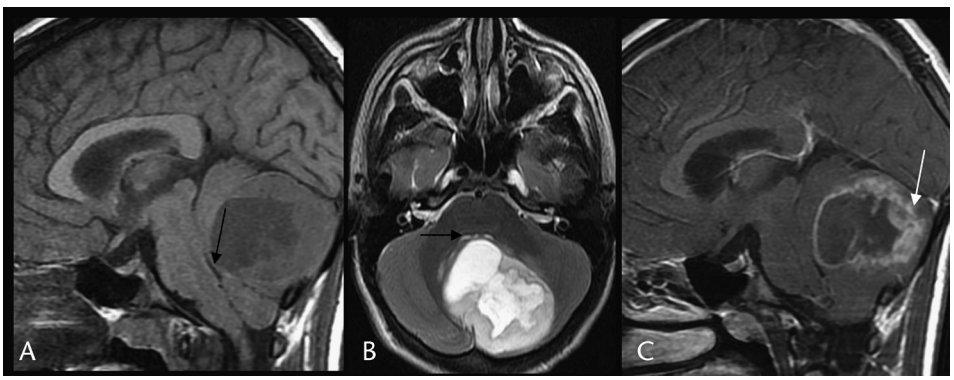

FIGURE 36. Cerebellar pilocytic astrocytoma. Sagittal T1 (A), axial T2 (B), and sagittal gadolinium T1 (C) images show a circumscribed vermian and left hemispheric cerebellar mass compressing the fourth ventricle (black arrows), displacing the cerebellar tonsils, and causing HC. The mass has T2-hyperintense cystic plus nodular and laminar solid components that show enhancement (white arrow).

© 2007 Lippincott Williams & Wilkins

Copyright © Lippincott Williams & Wilkins. Unauthorized reproduction of this article is prohibited.

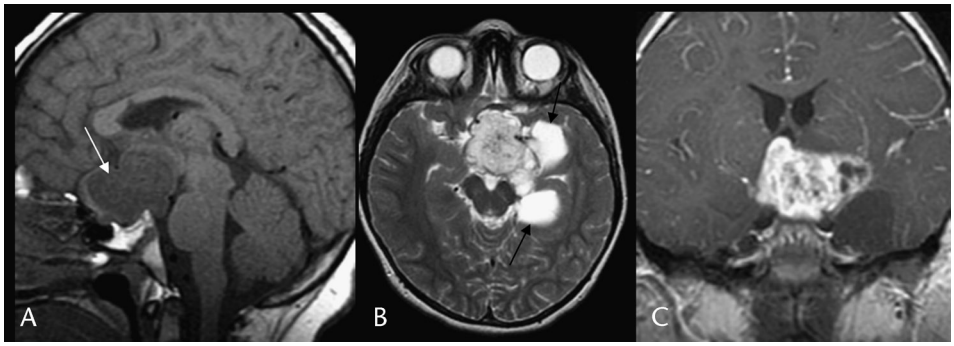

FIGURE 37. Optic-hypothalamic astrocytoma. Sagittal T1 (A), axial T2 (B), and coronal gadolinium T1 (C) images show a large mass (white arrow) that engulfs the optic chiasm, hypothalamus, and third ventricle. The mass is T2 isointense/hyperintense, enhances, and has some cystic components (black arrows) within the mesial left temporal lobe. There is mild ventriculomegaly.

neurofibromatosis 1, the diencephalic syndrome, or HC (Fig. 37). These masses are usually computed tomographic isodense/hypodense, T2 isointense/hyperintense, and often enhances. Craniopharyngioma is a common cystic and calcified tumor in this location but has a peak incidence in later childhood. Germ cell tumors commonly occur in the hypothalamic and pineal regions. Pineal GCTs often present with HC (Fig. 38). These tumors also have a propensity for seeding (Fig. 39). The most common type of GCT is the germinoma. Germinomas usually are small, well-defined lesions that are CT isodense/hyperdense, T2 isointense/hypointense, and markedly enhances. Larger and more heterogeneous lesions may represent nongerminomatous GCT (eg, choriocarcinoma, embryonal carcinoma, yolk sac tumor, teratoma, or mixed GCT). Pineoblastoma is also in the differential diagnosis. Teratoma is one of the most common tumors to occur in the first year of life. Fat, calcification, and cysts are characteristic (Fig. 38).[6,81,87–89]

SHUNT MALFUNCTION

Shunt malfunction, including shunt infection and obstruction, is suspected when there are symptoms and signs of acute ICP, seizures, or fever.[9,16,29] Shunt malfunction may occur as a result of catheter obstruction, disconnection, migration, or inadequate length for the growing child. The ventricular end of the catheter may be obstructed by choroid plexus or glial tissue if the catheter tip is not situated above and anterior to the foramen of Monro within the anterior body or frontal horn of the lateral ventricle. Catheter obstruction by ependymal or neural tissue may also occur with an extraventricular position or with ventricular collapse (embedded catheter). Shunt infection is a major cause of shunt malfunction. Shunt complications due to "overdrainage" include subdural hematomas or effusions, slit ventricle syndrome, craniosynostosis, and seizures. Distal ventriculovascular (eg, ventriculoatrial) shunt problems may include catheter or large-vessel thrombosis, endocarditis, embolism, arrhythmia, perforation, or detached tubing.[9] Ventriculoperitoneal distal shunt complications include hernia, hydrocele, ascites, cyst formation, intestinal volvulus and obstruction, viscus or peritoneal perforation, and neoplastic or infectious seeding.[9]

Initial imaging evaluation of shunt complications is usually done using CT, including a comparison with prior brain imaging exams. This includes an assessment of catheter

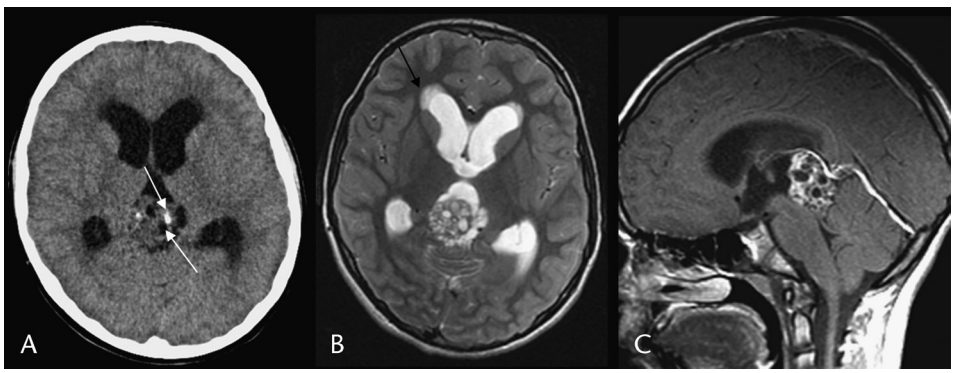

FIGURE 38. Mixed germ cell tumor with teratoma. Noncontrast CT (A) shows a heterogeneous pineal region mass with calcification and cysts (white arrows), but no fat. Hydrocephalus with edema is present. Axial T2 (B) and sagittal gadolinium T1 (C) images show a lobular cystic and solid mass that irregularly enhances. Third and lateral ventriculomegaly is present along with periventricular edema (black arrow). Biopsy of the mass was done during ETV.

© 2007 Lippincott Williams & Wilkins

Copyright © Lippincott Williams & Wilkins. Unauthorized reproduction of this article is prohibited.

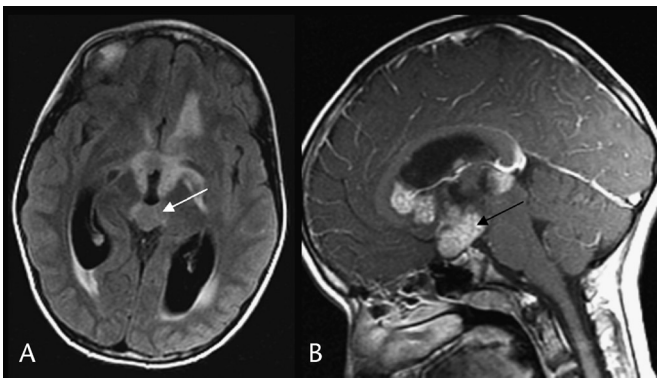

FIGURE 39. Multicentric, mixed germ cell tumor. Axial FLAIR (A) and sagittal gadolinium T1 (B) images show optic-hypothalamic (black arrow), pineal (white arrow), and bilateral periventricular isointense/hyperintense and enhancing nodular masses and HC with periventricular edema.

position, ventricular size and configuration, and any change thereof.[9] Findings or changes may include an obvious increase in ventricular size (Fig. 40); a more subtle increase in dilatation with rounding of the temporal horns, frontal horns, or third ventricle (Fig. 41); asymmetric or disproportionate ventricular dilatation; edema or cysts about the ventricles or along the catheter (Fig. 42); a decrease or loss of the sulci, fissures, or cisterns; reduced gray-white matter differentiation; a shift of the midline markers; or other signs of impending or frank herniation.

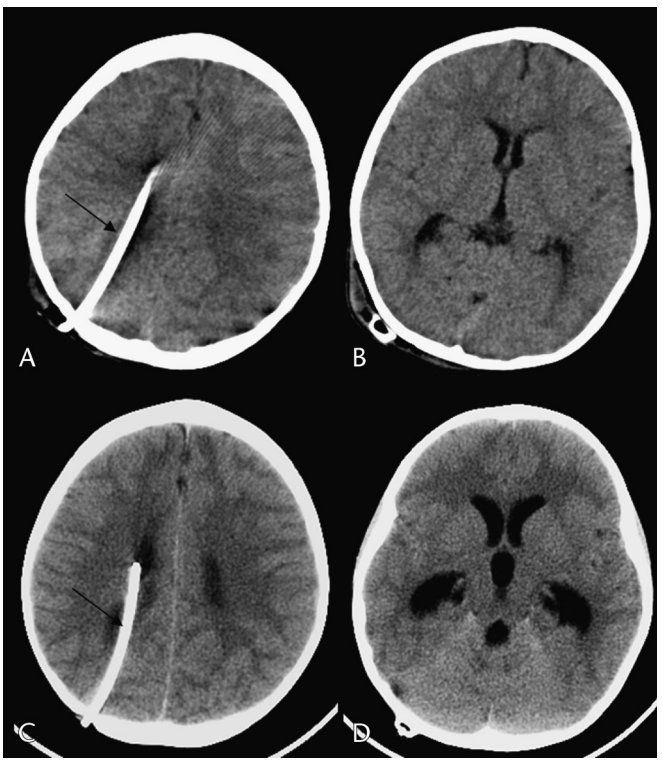

FIGURE 40. Shunt malfunction. Noncontrast CT images (A–B) at baseline. Noncontrast CT images (C–D) at presentation for shunt malfunction show that when compared with the previous baseline CT, the lateral and third ventricles have clearly increased in size, have a more rounded configuration, and there is a reduction in the sulci and fissures. A right parietal ventricular catheter is positioned along the upper body of the right lateral ventricle (black arrows).

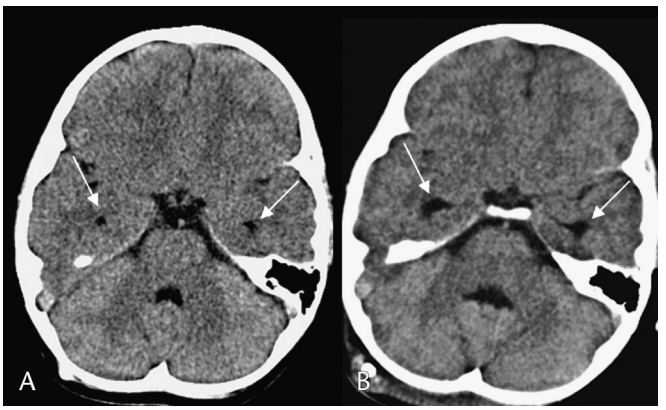

FIGURE 41. Shunt malfunction. Noncontrast CT (A) at baseline. Noncontrast CT (B) at presentation for shunt malfunction, in comparison with the previous baseline CT, shows only a slight increase in size of the temporal horns (arrows).

Along with brain CT, imaging often also includes shunt series radiographs (head and neck, thorax, abdomen, and pelvis) or US to evaluate for VP shunt system discontinuity and abdominal complications.[9,90] Ventricular shunt tap is occasionally necessary, whereas contrast shuntogram is rarely needed. Occasionally, CT with CSF contrast enhancement may be needed to evaluate the complex, encysted, or compartmentalized system to assist in proper drainage or shunt catheter placement. Isolation of the fourth ventricle may occur after lateral ventricular shunting due to secondary aqueductal closure in the presence of an existing outlet fourth ventricular obstruction (Fig. 43).[9] Expansion of the fourth ventricle results from continued choroid plexus CSF

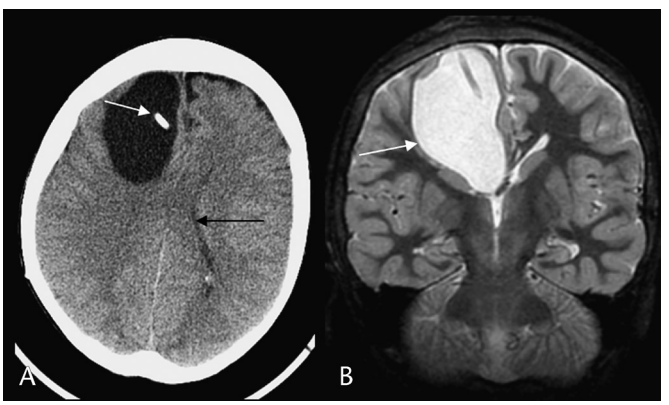

FIGURE 42. Pericatheter cyst. Noncontrast CT (A) shows a large right frontal low-density cyst along the ventricular catheter (white arrow) and small lateral ventricles (black arrow). Coronal short τ inversion recovery (B) image shows the relationship of the high-intensity pericatheter cyst (white arrow) to the small third and lateral ventricles.

© 2007 Lippincott Williams & Wilkins

Copyright © Lippincott Williams & Wilkins. Unauthorized reproduction of this article is prohibited.

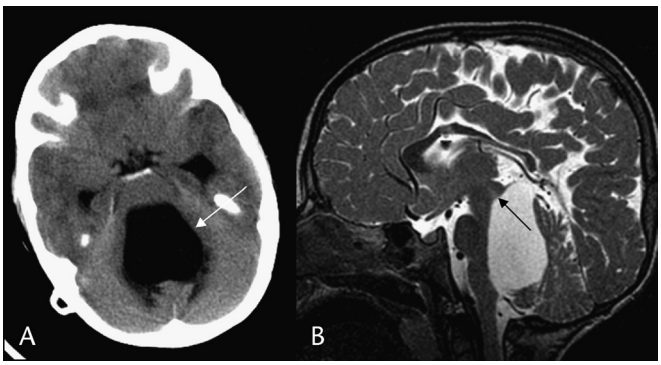

FIGURE 43. Isolated fourth ventricle in shunted PHH. Noncontrast CT (A) shows marked enlargement of the fourth ventricle (white arrow) with surrounding edema. Sagittal T2 (B) image further delineates the extent of the trapped fourth ventricle, including the deformation of the brain stem and cerebellum, the closed aqueduct (black arrow), and the small third and lateral ventricles.

production, and there may be progressive compression of the brain stem. Isolation of the fourth ventricle may be encountered after shunting of HC for Chiari II malformation or for shunting of outlet foraminal adhesive occlusion from infection or hemorrhage. Again, multiplanar MRI or CSF contrast-enhanced CT may assist in preoperative planning along with stereotactic techniques or intraoperative US guidance to facilitate catheter placement.

SUMMARY

Hydrocephalus is the end point of many different disease processes and is often found in infants and young children who are imaged to assess the common clinical presentations of macrocephaly and increased intracranial pressure. Familiarity with the common causes of HC, including posthemorrhage, postinfection, developmental anomalies, and masses (cysts and neoplasms) is important for the radiologist and technologists imaging and evaluating these patients. The radiologist can assist clinicians (including general pediatricians, neurologists, and neurosurgeons) in managing these patients, first by identifying the presence of HC, then assessing the underlying cause, directing the approach to treatment, and finally, by following results of treatment (especially after tumor resection and VP shunt placement or third ventriculostomy). Ultrasound, CT, and MR play unique roles in assessment of the infant with HC.

REFERENCES

1. Dias MS, Li V. Pediatric neurosurgical disease. *Pediatr Clin North Am*. 1998;45:1539–1578.
2. DeMyer W. Microcephaly, microcephaly, megalocephaly and megalencephaly. In: Swaiman K, ed. *Pediatric Neurology*. 2nd ed. St. Louis: Mosby; 1994;2:205–218.
3. Hamza M, Bodensteiner J, Noorani P, et al. Benign extracerebral fluid collections: a cause of macrocrania in infancy. *Pediatr Neurol*. 1987;3:218–221.
4. Maytal J, Alvarez L, Elkin C. External hydrocephalus: radiologic spectrum and differentiation from cerebral atrophy. *AJR Am J Roentgenol*. 1987;148:1223–1230.
5. Wilms G, Vanderschueren G, Demaerel PH, et al. CT and MR in infants with pericerebral collections and macrocephaly: benign enlargement of the subarachnoid spaces versus subdural collections. *AJNR Am J Neuroradiol*. 1993;14:855–860.
6. Barkovich AJ. *Pediatric Neuroimaging*. 4th ed. Philadelphia: Lippincott Williams and Wilkins; 2005.
7. Muenchberger H, Assaad N, Joy P, et al. Idiopathic macrocephaly in the infant: long-term neurological and neuropsychological outcome. *Childs Nerv Syst*. 2006;22:1242–1248.
8. Amodio J, Spektor V, Pramanik B, et al. Spontaneous development of bilateral subdural hematomas in an infant with benign infantile hydrocephalus: color Doppler assessment of vessels traversing extra-axial spaces. *Pediatr Radiol*. 2005;35:1113–1117.
9. Barnes P, Urion D, Share J. Clinical principles of pediatric neuroradiology. In: Wolpert S, Barnes P, eds. *MRI in Pediatric Neuroradiology*. St Louis: Mosby; 1992:71–78.
10. Trauner D. Increased intracranial pressure. In: Swaiman K, ed. *Pediatric Neurology*. 2nd ed. St Louis: Mosby; 1994;2:197–204.
11. Becker LE. Infections of the developing brain. *AJNR Am J Neuroradiol*. 1992;13:537–549.
12. Fitz CR. Inflammatory diseases of the brain in childhood. *AJNR Am J Neuroradiol*. 1992;13:551–568.
13. Flodmark O. Neuroradiology of selected disorders of the meninges, calvarium and venous sinuses. *AJNR Am J Neuroradiol*. 1992;13:483–492.
14. Harwood-Nash DC. Abuse to the pediatric central nervous system. *AJNR Am J Neuroradiol*. 1993;13:569–576.
15. Moser FG, Hilal SK, Abrams G. MR imaging of pseudotumor cerebri. *AJR Am J Roentgenol*. 1988;150:903–909.
16. Rorke LB, Zimmerman RA. Prematurity, postmaturity, and destructive lesions in utero. *AJNR Am J Neuroradiol*. 1992;13:517–536.
17. Carey CM, Tullous MW, Walker ML. Hydrocephalus: etiology, pathologic effects, diagnosis, and natural history. In: Cheek WR, ed. *Pediatric Neurosurgery*. 3rd ed. Philadelphia: WB Saunders; 1994:185–201.
18. Harwood-Nash D, Fitz C. Hydrocephalus. In: Harwood-Nash D, Fitz C, eds. *Neuroradiology in Infants and Children*. St Louis: Mosby; 1976; 2:609–667.
19. McComb JG. Cerebrospinal fluid physiology of the developing fetus. *AJNR Am J Neuroradiol*. 1992;13:595–600.
20. Naidich TP. Hydrocephalus. Paper presented at: Core Curriculum Course in Neuroradiology, 32nd Annual ASNR Meeting; May 1–2, 1993; Nashville, TN.
21. McLone DG, Naidich TP. Developmental morphology of the subarachnoid space, brain vasculature and contiguous structures, and the cause of the Chiari II malformation. *AJNR Am J Neuroradiol*. 1992;13:463–482.
22. Altman NR, Naidich TP, Braffman BH. Posterior fossa malformations. *AJNR Am J Neuroradiol*. 1992;13:691–724.
23. Naidich TP, Altman NR, Braffman BH, et al. Cephaloceles and related malformations. *AJNR Am J Neuroradiol*. 1992;13:655–690.
24. Barkovich AJ, Edwards MS. Applications of neuroimaging in hydrocephalus. *Pediatr Neurosurg*. 1992;18:65–83.
25. Gammal T, Allen M, Brooks B. MR evaluation of hydrocephalus. *AJR Am J Roentgenol*. 1987;149:807–813.
26. Quencer RM. Intracranial CSF flow in pediatric hydrocephalus: evaluation with cine-MR imaging. *AJNR Am J Neuroradiol*. 1992;13: 601–608.
27. Babcock D, Han B, Dine M. Sonographic findings in infants with macrocrania. *AJR Am J Roentgenol*. 1988;150:1359–1365.
28. Taylor GA, Madsen JR. Hemodynamic response to fontanelle compression in neonatal hydrocephalus. *Radiology*. 1996; 201:685.
29. Marlin AE, Gaskill SJ. Cerebrospinal fluid shunts: complications and results. In: Cheek WR, ed. *Pediatric Neurosurgery*. 3rd ed. Philadelphia: WB Saunders; 1994:221–233.
30. Rekate HL. Treatment of hydrocephalus. In: Cheek WR, ed. *Pediatric Neurosurgery*. 3rd ed. Philadelphia: WB Saunders; 1994: 202–220.
31. Etus V, Ceylan S. Success of endoscopic third ventriculostomy in children less than 2 years of age. *Neurosurg Rev*. 2005;28: 284–288.

© 2007 Lippincott Williams & Wilkins

Copyright © Lippincott Williams & Wilkins. Unauthorized reproduction of this article is prohibited.

32. Buxton N, Macarthur D, Mallucci C, et al. Neuroendoscopic third ventriculostomy in patients less than 1 year old. *Pediatr Neurosurg*. 1998;29:73–76.
33. Fritsch MJ, Mehdorn M. Endoscopic intraventricular surgery for treatment of hydrocephalus and loculated CSF space in children less than one year of age. *Pediatr Neurosurg*. 2002;36:183–188.
34. Ruggiero C, Cinalli G, Spennato P, et al. Endoscopic third ventriculostomy in the treatment of hydrocephalus in posterior fossa tumors in children. *Childs Nerv Syst*. 2004;20:828–833.
35. Fritsch MJ, Doerner L, Kienke S, et al. Hydrocephalus in children with posterior fossa tumors: role of endoscopic third ventriculostomy. *J Neurosurg*. 2005;103(suppl 1):40–42.
36. Peretta P, Ragazzi P, Carlino CF, et al. The role of Ommaya reservoir and endoscopic third ventriculostomy in the management of post-hemorrhagic hydrocephalus of prematurity. *Childs Nerv Syst*. 2007;23:765–771.
37. O'brien DF, Seghedoni A, Collins DR, et al. Is there an indication for ETV in young infants in aetiologies other than isolated aqueductal stenosis? *Childs Nerv Syst*. 2006;22:1565–1572.
38. Takahashi Y. Long-term outcome and neurologic development after third ventriculostomy versus shunting during infancy. *Childs Nerv Syst*. 2006;22:1591–1602.
39. Kulkarni AV, Drake JM, Armstrong DC, et al. Imaging correlates of successful endoscopic third ventriculostomy. *J Neurosurg*. 2000;92: 915–919.
40. Nowoslawska E, Polis L, Kaniewska D, et al. Influence of neuroendoscopic third ventriculostomy on the size of ventricles in chronic hydrocephalus. *J Child Neurol*. 2004;19:579–587.
41. Fischbein NJ, Ciricillo SF, Barr RM, et al. Endoscopic third ventriculostomy: MR assessment of patency with 2-D cine phase-contrast versus T2-weighted fast spin echo technique. *Pediatr Neurosurg*. 1998;28:70–78.
42. Kazan S, Gura A, Ucar T, et al. Hydrocephalus after intraventricular hemorrhage in preterm and low-birth weight infants: analysis of associated risk factors for ventriculoperitoneal shunting. *Surg Neurol*. 2005;S2:77–81.
43. Garton HJL, Piatt JH. Hydrocephalus. *Pediatr Clin N Am*. 2004;51: 305–325.
44. Laroche JC. Posthemorrhagic hydrocephalus in infancy. *Biol Neonate*. 1972;20:287–299.
45. Baker LL, Stevenson DK, Enzmann DR. End-stage periventricular leukomalacia: MR evaluation. *Radiology*. 1988;168:809–815.
46. Keeney SE, Adcock EW, McArdle CB. Prospective observations of 100 high-risk neonates by high-field (1.5Tesla) magnetic resonance imaging of the central nervous system. II. Lesions associated with hypoxic-ischemic encephalopathy. *Pediatrics*. 1991;87:431–438.
47. Skranes JS, Nilsen G, Olaug S, et al. Cerebral MRI of very low birth weight children at 6 years of age compared with the findings at 1 year. *Pediatr Radiol*. 1998;28:471–475.
48. Jhawar BS, Ranger A, Steven D. Risk factors for intracranial hemorrhage among full-term infants: a case control study. *Neurosurgery*. 2003;52: 581–588.
49. Grossman R, Novak G, Patel M, et al. MRI in neonatal dural sinus thrombosis. *Pediatr Neurol*. 1993;9:235–238.
50. DeVeber G, Andrew M, Adams C, et al. Cerebral sinovenous thrombosis in children. *N Engl J Med*. 2001;345:417–423.
51. Lynch JK, Hirtz DG, DeVeber G, et al. Report of the National Institute of Neurologic Disorders and Stroke Workshop on Perinatal and Childhood Stroke. *Pediatrics*. 2002;109:116–123.
52. Carvalho KS, Bodensteiner JB, Connolly PJ, et al. Cerebral venous thrombosis in children. *J Child Neurol*. 2001;16:574–580.
53. Bale J. Congenital infections. *Neurol Clin N Am*. 2002;20: 1039–1060.
54. Barkovich AJ, Lindan CE. Congenital cytomegalovirus infection of the brain: imaging analysis and embryologic considerations. *AJNR Am J Neuroradiol*. 1994;15:703–715.
55. Boesch C, Issakainen J, Kewitz G, et al. Magnetic resonance imaging of the brain in congenital cytomegalovirus infection. *Pediatr Radiol*. 1989;19:91–93.
56. Barnes PD, Poussaint TY, Burrows PE: Imaging of pediatric central nervous system infections. *Neuroimaging Clin N Am*. 1994;4: 367–391.
57. Bell WE. Bacterial meningitis in children: selected aspects. *Pediatr Clin North Am*. 1992;39:651–668.
58. Chang KH, Han MH, Roh JK, et al. Gd-DTPA-enhanced MR imaging of the brain in patients with meningitis: comparison with CT. *Am J Neuroradiol*. 1990;11:69–76.
59. Chang KH, Han MH, Roh JK, et al. Gd-DTPA-enhanced MR imaging in intracranial tuberculosis. *Neuroradiology*. 1990;32:19–25.
60. Stevenson KL. Chiari II malformation: past, present and future. *Neurosurg Focus*. 2004;16:E5.
61. Curnes JT, Oakes WJ, Boyko OB. MR imaging of hindbrain deformity in Chiari II patients with and without symptoms of brainstem compression. *Am J Neuroradiol*. 1989;10:293–302.
62. Naidich TP, Pudlowski RM, Naidich JB. Computed tomographic signs of the Chiari II malformation. III: ventricles and cisterns. *Radiology*. 1980;134:657–663.
63. Naidich TP, McLone DG, Fulling KH. The Chiari II malformation: Part IV. The hindbrain deformity. *Neuroradiology*. 1983;25: 179–197.
64. Barkovich AJ, Kjos BO, Norman D, et al. Revised classification of posterior fossa cysts and cystlike malformations based on the results of multiplanar MR imaging. *AJR Am J Roentgenol*. 1989;153: 1289–1300.
65. Strand RD, Barnes PD, Poussaint TY, et al. Cystic retrocerebellar malformations: unification of the Dandy-Walker complex and Blake's pouch cyst. *Pediatr Radiol*. 1993;28:258–260.
66. Calabro F, Arcuri T, Jinkins JR. Blake's pouch cyst: an entity within the Dandy-Walker continuum. *Neuroradiology*. 2000;42: 290–295.
67. Jellinger G. Anatomopathology of non-tumoral aqueductal stenosis. *J Neurosurg Sci*. 1986;30:1–16.
68. Barkovich AJ, Newton TH. MR of aqueductal stenosis: evidence of a broad spectrum of tectal distortion. *AJNR Am J Neuroradiol*. 1989;10: 471–476.
69. Pollack IF, Pang D, Albright AL. The long-term outcome in children with late-onset aqueductal stenosis resulting from benign intrinsic tectal tumors. *J Neurosurg*. 1994;80:681–688.
70. Boydston WR, Sanford RA, Muhlbauer MS, et al. Gliomas of the tectum and periaqueductal region of the mesencephalon. *Pediatr Neurosurg*. 1991–1992;17:234–238.
71. Osborn AG, Preece MT. Intracranial cysts: radiologic-pathologic correlation and imaging approach. *Radiology*. 2006;239:650–664.
72. Donaldson JW, Edwards-Brown M, Luerssen TG. Arachnoid cyst rupture with concurrent subdural hygroma. *Pediatr Neurosurg*. 2000;32:137–139.
73. Parsch CS, Krauss J, Hofmann E, et al. Arachnoid cysts associated with subdural hematomas and hygromas: analysis of 16 cases, long-term follow-up and review of the literature. *Neurosurgery*. 1997;40: 483–490.
74. Tamburrini G, Caldarelli M, Massimi L, et al. Subdural hygroma: an unwanted result of Sylvian arachnoid cyst marsupialization. *Childs Nerv Syst*. 2003;19:159–165.
75. Chen S, Ikawa F, Kurisu K, et al. Quantitative MR evaluation of intracranial epidermoid tumors by fast fluid-attenuated inversion recovery imaging and echo-planar diffusion-weighted imaging. *Am J Neuroradiol*. 2001;22:1089–1096.
76. Isaacs H. II. Perinatal brain tumors: a review of 250 cases. *Pediatr Neurol*. 2002;27:333–342.
77. Coates TL, Hinshaw DB Jr, Peckman N, et al. Pediatric choroid plexus neoplasms: MR, CT, and pathologic correlation. *Radiology*. 1989;173:81–88.
78. Meyers SP, Khademian ZP, Chuang SH, et al. Choroid plexus carcinomas in children: MRI features and patient outcomes. *Neuroradiology*. 2004;46:770–780.
79. Nagib MG, O'Fallon MT. Lateral ventricle choroid plexus papilloma in childhood: management and complications. *Surg Neurol*. 2000;54: 366–372.
80. Kumar R, Singh S. Childhood choroid plexus papillomas: operative complications. *Childs Nerv Syst*. 2005;21:138–143.
81. Isaacs H. I. Perinatal brain tumors: a review of 250 cases. *Pediatr Neurol*. 2002;27:249–261.
82. Vezina LG, Packer RJ. Infratentorial brain tumors of childhood. *Neuroimaging Clin N Am*. 1994;4:423–436.

© 2007 Lippincott Williams & Wilkins

Copyright © Lippincott Williams & Wilkins. Unauthorized reproduction of this article is prohibited.

83. Zimmerman RA, Bilaniuk LT, Rebsamen S. Magnetic resonance imaging of pediatric posterior fossa tumors. *Pediatr Neurosurg*. 1992;18:58–64.
84. Meyers SP, Kemp SS, Tarr RW. MR imaging features of medulloblastomas. *AJR Am J Roentgenol*. 1992;158:859–865.
85. Lefton DR, Pinto RS, Martin SW. MRI features of intracranial and spinal ependymomas. *Pediatr Neurosurg*. 1998;28:97–105.
86. Bambakidis NC, Robinson S, Cohen M, et al. Atypical teratoid/rhabdoid tumors of the central nervous system: clinical, radiographic and pathologic features. *Pediatr Neurosurg*. 2002;37:64–70.
87. Smirniotopoulos JG, Rushing EJ, Mena H. Pineal region masses: differential diagnosis. *Radiographics*. 1992;12:577–596.
88. Tien R, Barkovich A, Edwards M. MR imaging of pineal tumors. *AJR Am J Roentgenol*. 1990;155:143–151.
89. Ambrosino M, Hernanz-Schulman M, Genieser N, et al. Brain tumors in infants less than a year of age. *Pediatr Radiol*. 1988; 19:6–8.
90. Grunebaum M, Ziv N, Kornreich L, et al. The sonographic signs of the peritoneal pseudocyst obstructing the ventriculoperitoneal shunt in children. *Neuroradiology*. 1988;30:433–438.

© 2007 Lippincott Williams & Wilkins

Copyright © Lippincott Williams & Wilkins. Unauthorized reproduction of this article is prohibited.